Combined paleomagnetic, isotopic, and stratigraphic evidence for true polar wander from the Neoproterozoic Akademikerbreen Group, Svalbard, Norway

Adam C. Maloof[†]
Galen P. Halverson[‡]
Department of Earth and Planetary Sciences, Harvard University, 20 Oxford Street, Cambridge, Massachusetts 02138, USA

Joseph L. Kirschvink
Division of Geological and Planetary Sciences, California Institute of Technology 170-25, 1200 East California Boulevard, Pasadena, California 91125, USA

Daniel P. Schrag
Department of Earth and Planetary Sciences, Harvard University, 20 Oxford Street, Cambridge, Massachusetts 02138, USA

Benjamin P. Weiss
Department of Earth, Atmospheric and Planetary Sciences, Massachusetts Institute of Technology, 77 Massachusetts Avenue, Cambridge, Massachusetts 02139, USA

Paul F. Hoffman
Department of Earth and Planetary Sciences, Harvard University, 20 Oxford Street, Cambridge, Massachusetts 02138, USA

ABSTRACT

We present new paleomagnetic data from three Middle Neoproterozoic carbonate units of East Svalbard, Norway. The paleomagnetic record is gleaned from 50 to 650 m of continuous, platformal carbonate sediment, is reproduced at three locations distributed over >100 km on a single craton, and scores a 5–6 (out of 7) on the Van der Voo (1990) reliability scale. Two >50° shifts in paleomagnetic direction are coincident with equally abrupt shifts in $\delta^{13}C$ and transient changes in relative sea level. We explore four possible explanations for these coincidental changes: rapid plate tectonic rotation during depositional hiatus, magnetic excursions, nongeocentric axial-dipole fields, and true polar wander. We conclude that the observations are explained most readily by rapid shifts in paleogeography associated with a pair of true polar wander events. Future work in sediments of equivalent age from other basins can test directly the true polar wander hypothesis because this type of event would affect every continent in a predictable manner, depending on the continent's changing position relative to Earth's spin axis.

Keywords: polar wandering, paleomagnetism, Svalbard, Neoproterozoic, carbon cycle, paleogeography.

INTRODUCTION

Earth's equilibrium figure is dominated by a 20-km-amplitude equatorial bulge related to the latitudinal dependence of gravity on a rotating spheroid. This hydrostatic bulge adjusts to changes in the position of Earth's spin vector in ~10^4–10^6 yr, the characteristic time scale for mantle deformation in response to long-wavelength loading (Ranalli, 1995; Steinberger and O'Connell, 1997). On a hydrostatic planet, over time scales ~10^6 yr, the rotational bulge exerts little or no stabilizing effect on the orientation of the spin vector with respect to the solid Earth (Goldreich and Toomre, 1969; Steinberger and O'Connell, 1997, 2002; Richards et al., 1997). Depending on the effective elastic thickness and viscous relaxation time of the lithosphere, and the ability of plate boundaries to consume strain, the presence of viscoelastic lithosphere may prevent perfect relaxation of the hydrostatic bulge, leaving remnants of previous rotational flattening to stabilize the spin vector (Willemann, 1984; Matsuyama et al., 2006).

Buoyancy-driven rising and sinking of mantle density heterogeneities cause deflections in compositional discontinuity surfaces such as the core-mantle boundary, the 660 km discontinuity, and Earth's surface, inducing perturbations to Earth's nonhydrostatic inertia tensor (that is, with the contribution from the hydrostatic rotational bulge removed) (Steinberger and O'Connell, 1997, 2002; Spada et al., 1992; Sabadini and Yuen, 1989; Richards and Hager, 1984; Ricard et al., 1993). Changes in Earth's nonhydrostatic inertia tensor cause motion of the solid Earth with respect to the spin vector until the maximum principal inertia axis (I_{max}) is aligned with the spin vector. True polar wander refers to the relative motion between the spin vector and the solid Earth, where the spin vector and hydrostatic bulge remain fixed in a celestial reference frame, and the solid Earth is deformed through the rotational bulge as if through a standing wave (Evans, 2003). Both paleomagnetic (Besse and Courtillot, 1991, 2002) and

[†]Present address: Department of Geosciences, Princeton University, 217 Guyot Hall, Washington Road, Princeton, New Jersey 08544, USA; e-mail: maloof@princeton.edu.
[‡]Present address: UMR 5563, Laboratoire des Mécanismes et Transferts en Géologie (LMTG), Université Paul Sabatier, 14 avenue Edouard Belin, 31400 Toulouse, France.

GSA Bulletin; September/October 2006; v. 118; no. 9/10; p. 1099–1124; doi: 10.1130/B25892.1; 11 figures; 3 tables.

modeling (Steinberger and O'Connell, 1997) studies have found 5–20° of true polar wander over the past 10^7 yr, a relatively modest amount of true polar wander to complement the apparent polar wander (APW) due to plate tectonics. This slow rate of TPW may have been controlled by relatively high lower mantle viscosities (Steinberger and O'Connell, 1997) and the particular geometry of loads relative to the nonhydrostatic inertia tensor (Richards et al., 1997).

Inertial interchange true polar wander is a type of true polar wander that may occur when normal advection of mantle density heterogeneities causes changes in the relative magnitudes (rather than orientations) of the principal inertia axes. If a threshold internal density structure is reached where I_{max} becomes less than the intermediate inertial axis I_{int}, then the entire silicate Earth will rotate quickly around I_{min} until the new I_{max} is aligned with the spin vector (Fisher, 1974).

Because I_{max}, I_{int}, and I_{min} are by definition orthogonal, the simplest form of inertial interchange true polar wander will result in a 90° interchange of inertial axes where continents farthest from I_{min} undergo the largest latitudinal excursions (Fisher, 1974; Kirschvink et al., 1997). However, depending on the uncompensated-size and geographic location of the true polar wander–inducing load with respect to the remnant equatorial bulge, an inertial interchange true polar wander event may lead to rotations less than 90° (Matsuyama et al., 2006). In principle, a series of three paleomagnetic poles spanning an inertial interchange true polar wander event from any individual continent should fall on a great circle, with the pole to that great circle approximating I_{min} (Evans, 1998, 2003).

The rate of true polar wander depends critically on the viscosity structure of the mantle, which determines (1) the rate at which nonhydrostatic (i.e., imperfectly compensated) mass anomalies may be imposed, and (2) the rate at which Earth's rotational bulge can readjust to the changing rotation axis. For a modern Earth viscosity structure derived from studies of glacio-isostatic rebound and the geoid (e.g., Hager and Clayton, 1989), it has been found that a full 90° of inertial interchange true polar wander would take 3–20 m.y. (Steinberger and O'Connell, 1997, 2002).

Because there is a lag between the instantaneous response of the world ocean and the delayed response of the viscoelastic mantle-lithosphere system, true polar wander will cause transient sea-level change observable on continental shelves (Darwin, 1877; Gold, 1955; Sabadini et al., 1990; Mound and Mitrovica, 1998; Mound et al., 1999, 2001, 2003). For example, a continental shelf driven toward lower latitude (moving away from the spin vector) would experience sea-level rise as the ocean adjusts instantly to the weaker gravitational potential at lower latitudes and the mantle-lithosphere lags. When the true polar wander event is complete, the load on the mantle-lithosphere is removed, and the mantle-lithosphere adjusts to equilibrium form, returning sea level to its approximate initial state. For a typical mantle viscosity structure and effective elastic lithospheric thickness, 90° of true polar wander–induced latitudinal motion over 10–30 m.y. will cause 50 to >200 m of local sea-level change (Mound et al., 1999).

Little work has been done to evaluate the possible influence of rapid true polar wander on the biosphere, the global carbon cycle, and the architecture of stratigraphic records spanning a true polar wander event. In this contribution, we present a paleomagnetic, carbon isotopic, and stratigraphic record from Middle Neoproterozoic carbonate rocks in Svalbard, Norway, and generate a testable hypothesis linking $\delta^{13}C$ shifts and transient sea-level changes to a latitudinal redistribution of the continents possibly associated with a pair of rapid true polar wander events.

TRUE POLAR WANDER OBSERVED?

Seasonal redistribution of atmospheric and ocean mass (12 month period) along with free Eulerian precession of a rotating deformable body (14 month period) drive periodic true polar wander (known as the Chandler Wobble) with an amplitude of 1000–1500 cm/cycle (e.g., Stacey, 1992). Astronomical observations over the last century have recognized secular true polar wander superimposed on the Chandler Wobble with a rate of ~10 cm/yr toward 80°W longitude (after correction for plate tectonic motion) (e.g., Vermeersen and Sabadini, 1999). The redistribution of mass associated with Holocene deglaciation and isostatic rebound is thought to be the dominant cause of this recent secular true polar wander (Nakiboglu and Lambeck, 1980; Sabadini and Peltier, 1981; Sabadini et al., 1982; Wu and Peltier, 1984; Bills and James, 1996; Peltier, 1998; Vermeersen and Sabadini, 1999; Mitrovica et al., 2005). Depending on the viscosity structure of the mantle, 0.1–1.0° of true polar wander is thought to be possible during a 10–20 k.y. deglaciation. Although Holocene and Pliocene-Pleistocene true polar wander rates are similar to or greater than average seafloor spreading rates, ~40–100-k.y.-long glacial-interglacial excitation of polar wander appears to have driven <5° of secular true polar wander over the past 5 m.y. (Andrews, 1985; Schneider and Kent, 1986).

Assuming that hotspots are fixed with respect to each other and with respect to Earth's spin axis, paleorates of true polar wander are calculated by subtracting a continent's hotspot-track–derived motion from its apparent polar wander–derived motion (Morgan, 1981; Evans, 2003). Fixed-hotspot studies using different filters on the global paleomagnetic database have suggested mean Cenozoic-Mesozoic true polar wander rates of 1–5 cm/yr, and a total of 5–20° of secular true polar wander over the last ~200 m.y. (e.g., Livermore et al., 1984; Andrews, 1985; Besse and Courtillot, 1991; Prévot et al., 2000). Depending on how the global paleomagnetic database is filtered, some of the most recent analyses suggest episodic bursts of true polar wander, with almost zero true polar wander from 0 to 80 Ma and 150 to 200 Ma, but rapid true polar wander events from 80 to 150 Ma (Besse and Courtillot, 2002; Prévot et al., 2000). However, recent work has suggested that hotspots may not be fixed with respect to Earth's spin axis or with respect to each other (Tarduno and Gee, 1995; Cande et al., 1995; Tarduno and Cottrell, 1997; Steinberger and O'Connell, 1998; DiVenere and Kent, 1999; Steinberger et al., 2004), making such predictions suspect at best.

Methods that attempt to quantify common motion between continents due to true polar wander without relying on a fixed-hotspot reference frame do not produce statistically significant amounts of true polar wander since the Cretaceous, although uncertainties are large (McKenzie, 1972; McElhinny, 1973; Jurdy and Van der Voo, 1974, 1975). Sager and Koppers (2000) used disparate paleomagnetic poles from Pacific seamounts of indistinguishable $^{40}Ar/^{39}Ar$ age to suggest an episode of rapid true polar wander ca. 84 ± 2 Ma. However, Cottrell and Tarduno (2000) suggested that the poles recalculated by Sager and Koppers (2000) from seamount magnetic anomaly models were not sufficiently accurate to confidently isolate true polar wander. Furthermore, paleomagnetic data from Late Cretaceous pelagic limestones of the Umbrian Apennines do not show any magnetostratigraphic evidence for true polar wander (Alvarez and Lowrie, 1978; Rocchia et al., 1990; Uno and Bice, 2001).

Attempts to quantify true polar wander episodes during pre-Mesozoic intervals in Earth history, when hotspot tracks in ocean crust are not available, have been met with no less controversy. Marcano et al. (1999) considered the ~35° of rotation experienced by Pangea between 295 and 205 Ma and suggested that the lack of subduction along the leading edge of Pangea (northern Laurentia, Baltica, and Siberia) could mean that much of this paleomagnetic rotation was accomplished by true polar wander. Van der Voo (1994) recognized that the Late Ordovician–Late Devonian polar wander paths of Laurentia, Baltica, Gondwana, and possibly South China

and Siberia, have similar "looping shapes." He suggested that ~75° of cumulative true polar wander may have occurred over ~75 m.y., and that true polar wander may have been relatively more important than plate tectonics during this interval. Kirschvink et al. (1997) proposed ~90° of inertial interchange true polar wander during the Early–Middle Cambrian based on a quality-filtered version of the global paleomagnetic database. The selection of Cambrian paleomagnetic poles has been debated vigorously, and the evidence for true polar wander is considered ambiguous (Torsvik et al., 1998; Evans et al., 1998; Meert, 1999). Nevertheless, Evans (1998) recognized that the conditions prerequisite for a single rapid true polar wander event likely reflect long-lived mass distributions in the mantle that could lead to multiple, oscillatory true polar wander events. Evans (2003) went on to suggest that the large apparent polar wander motions affecting many continents from the Ediacaran to Early Carboniferous (635–350 Ma) may have been due to oscillatory true polar wander around a long-lived geoid high.

The unifying theme in these assessments of true polar wander from Paleozoic and Ediacaran time is that they all rely on correlation of paleomagnetic poles of variable quality and age uncertainty from different rock types and different continents. As Cottrell and Tarduno (2000) recognized, perhaps the most powerful test of any true polar wander hypothesis is paleomagnetic data from continuous sedimentary successions. Strik et al. (2003) observed a ~27° paleolatitudinal shift across an erosional surface in interbedded basalt flows and tuffs of the Late Archean Fortescue Group, West Australia. Other similar erosional surfaces within the same stratigraphic section did not record paleomagnetic shifts. New sensitive high-resolution ion microprobe (SHRIMP) U/Pb dates from felsic tuffs below (2721 ± 3 Ma) and above (2718 ± 3 Ma) the paleomagnetic shift suggest minimum rates of paleolatitudinal motion of 34 cm/yr (Blake et al., 2004). Strik et al. (2003) considered the possibility that the shift reflects an episode of rapid true polar wander or insufficient averaging of paleomagnetic secular variation, but favored an interpretation involving very fast plate tectonic motions over the maximum interval of time allowed by the U/Pb data. A true polar wander origin for the ~27° paleolatitudinal shift could be tested by finding a sedimentary succession of similar age on another continent, such as Ventersdorp Supergroup of southern Africa (e.g., South African Committee for Stratigraphy, 1980; Van der Westhuizen and Meintjes, 1991; Martin et al., 1998) or the Belingwe greenstone belt in Zimbabwe (e.g., Bickle et al., 1975; Martin et al., 1993).

New Observations from Svalbard

From 1999 to 2004, we conducted geologic field work in Svalbard, Norway (Fig. 1), aimed at building a high-resolution Neoproterozoic $\delta^{13}C$ curve in the framework of detailed mapping and sequence stratigraphy (Halverson et al., 2004, 2005). As part of this project, paleomagnetic sampling was undertaken to determine the changing latitude of Svalbard through the $\delta^{13}C$ fluctuations and glaciations of the Neoproterozoic. In this contribution, we present new paleomagnetic data from Svalbard that suggests a pair of rapid polar wandering or geomagnetic events at ca. 800 Ma. Our paleomagnetic record is extracted from 50 to 650 m of continuous (i.e., no covered intervals or correlations between outcrops), early-cemented platformal carbonate sediment, and it is reproduced at three locations distributed over >100 km on a single craton, implying that correlation, secular variation, inclination shallowing, tectonic rotation, and uncertainty of paleohorizontal do not contribute significant error. We link predicted changes in paleogeography derived from the paleomagnetic data to transient sea-level variations and long-term carbon-isotope shifts observed in the same stratigraphic records from Svalbard. We explore four possible explanations for these coincidental changes: rapid plate tectonic rotation during depositional hiatus, magnetic excursions, departure from a geocentric axial-dipole magnetic field, and true polar wander, and conclude that true polar wander may provide the most parsimonious interpretation of the data. We also show that the Svalbard data are consistent with the episode of true polar wander suggested by Li et al. (2004), which was based on disparate paleomagnetic poles from South China at 802 ± 10 and 748 ± 12 Ma.

GEOLOGIC SETTING

The Svalbard archipelago is located on the northwestern edge of the Barents shelf (Fig. 1A) and is composed of three tectonic terranes (Fig. 1B), juxtaposed by sinistral transpression during the Silurian-Devonian Ny Friesland orogeny (Harland and Gayer, 1972; Harland et al., 1992; Gee and Page, 1994; Lyberis and Manby, 1999; Dewey and Strachan, 2003). The northern part of the eastern terrane (Fig. 1C) is referred to as the Barentsian craton (ES) and contains northeast Spitsbergen, Nordaustlandet, and part of the Barents Sea (Fig. 1A) (Breivik et al., 2002). Barentsia is blanketed by a thick package of Neoproterozoic-Ordovician sedimentary rocks known as the Hecla Hoek succession. The remarkable similarity between the sedimentary records of the Hecla Hoek succession and the Eleanore Bay–Tillite succession of the southern East Greenland Caledonides has led to the interpretation that Barentsia was located along the Laurentian margin (Harland and Gayer, 1972) and formed part of a joint East Greenland–East Svalbard platform during the Neoproterozoic (Halverson et al., 2004).

The East Greenland–East Svalbard platform likely owed its origin to the separation of Amazonia, Baltica, and a northern continent from the eastern margin of Laurentia during the fragmentation of the Rodinia supercontinent. Based on the age of rift-to-drift successions on conjugate margins, it is generally agreed that Amazonia separated from Laurentia to form the southern Iapetus paleo-ocean ca. 550 Ma (Cawood et al., 2001), while a northern craton (possibly Siberia [Long, 1989; Surlyk, 1991] or North China) separated from the North Greenland margin ca. 520 Ma. Until recently, it was assumed that the ca. 615 Ma mafic Egersund dikes of SW Norway and Long Range dikes of western Newfoundland marked the separation of the Caledonian margins of Baltica and Laurentia (Bingen et al., 1998; Svenningsen, 2001). However, Hartz and Torsvik (2002) noted the greater similarity between sedimentary successions of the southern peri-Urals and East Greenland–East Svalbard and suggested inverting Baltica (given the lack of polarity constraints on the paleomagnetic data, a 180° inversion of Baltica is still a viable paleogeographic solution). In this reconstruction, the southern peri-Urals East Greenland–East Svalbard basin would have developed as a Middle Neoproterozoic sinistral pull-apart basin related to the opening of the Ran Sea between Baltica and Amazonia (Hartz and Torsvik, 2002). This scenario is consistent with the deposition of 4 km of Veteranen Group siliciclastic sediments during active extension, followed by 2 km of shallow-water Akademikerbreen Group carbonates during subsequent thermally driven subsidence (Fig. 1D). The tropical latitude of East Svalbard (see following) and lack of terrigenous sediments within the carbonate succession suggest that the southern peri-Urals East Greenland–East Svalbard basin became an isolated platform like the Bahamas, or a promontory like Florida, that was devoid of major rivers during the thermal subsidence phase.

Akademikerbreen Group carbonates are characterized by strongly enriched mean values of $\delta^{13}C$, ~5‰ (Fig. 1D), and mark the longest interval in Earth history dominated by such positive $\delta^{13}C$ (Knoll et al., 1986; Halverson et al., 2005). A prominent exception to this rule occurs in the Upper Grusdievbreen and Lower Svanbergfjellet Formations, where $\delta^{13}C$ varies between –3‰ and 0.5‰ through ~325 m of stratigraphy (Fig. 1D). This low $\delta^{13}C$ interval is referred to as the Bitter Springs Stage after its counterpart in the Bitter

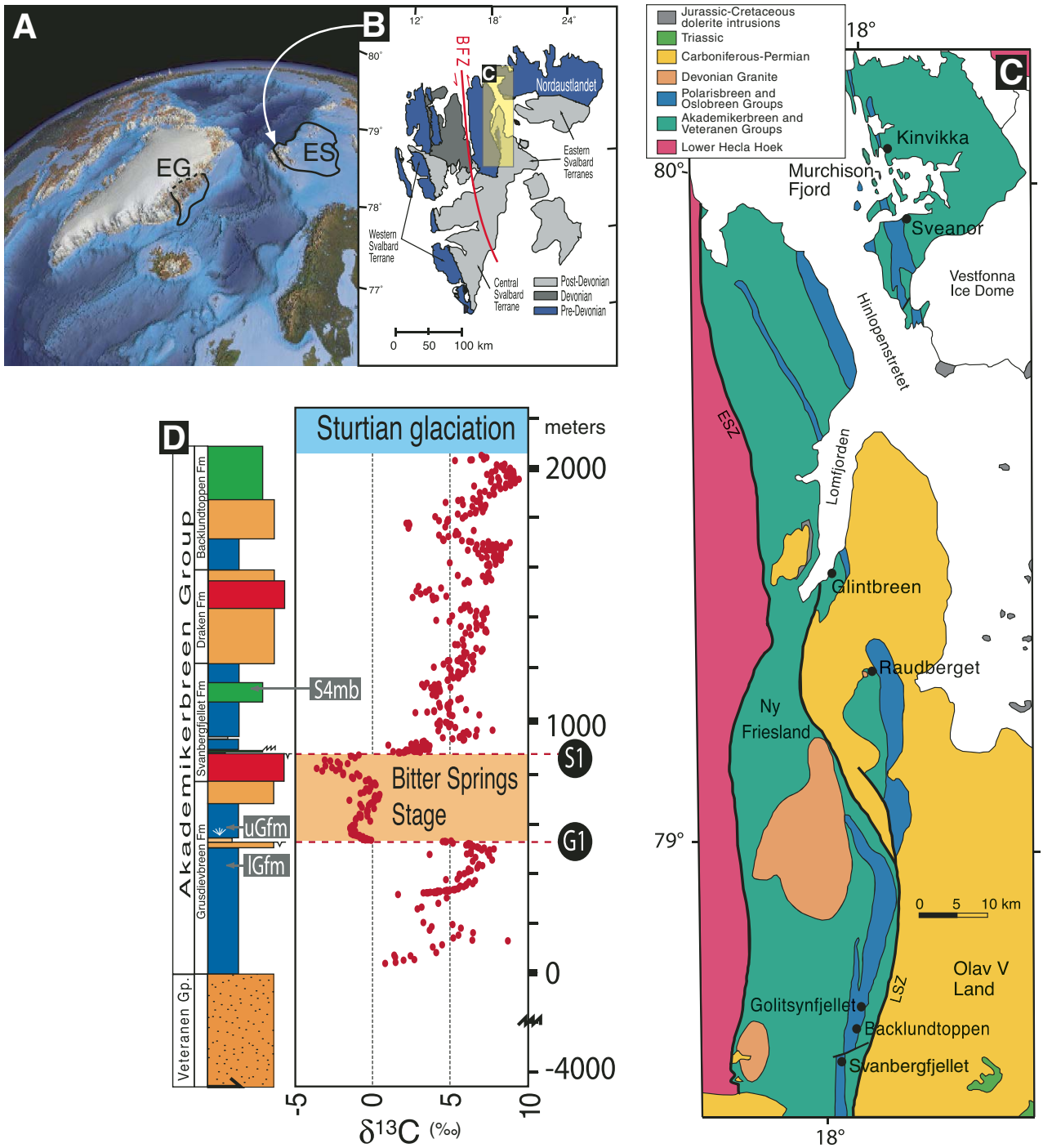

Figure 1. (A) The Svalbard archipelago is located on the northwest edge of the Barents Shelf and is composed of (B) three distinct tectonic terranes (western, central, and eastern), which were juxtaposed via sinistral transpression along the Billefjorden (BFZ) and other north-south fault zones during Silurian-Devonian times. East Greenland (EG) and East Svalbard (ES, also known as Barentsia) are thought to have been part of a contiguous Neoproterozoic basin (EGES) in Eastern Laurentia (A). The semitransparent yellow box in B marks the coverage of the generalized geologic map in C, after Harland (1997), which shows the locations of our measured stratigraphic sections through the Akademikerbreen Group that are mentioned in the text. In C, note the positions of (1) the Cretaceous sills west of Glintbreen, (2) the small Devonian intrusion west of Raudberget, and (3) the Lomfjorden shear zone (LSZ) east of Backlundtoppen, and (4) the Eolusseltta shear zone (ESZ) separating Lower Hecla Hoek metamorphic rocks to the west from Neoproterozoic rocks to the east. (D) A composite stratigraphic section (see Fig. 7 for a key to the carbonate lithostratigraphy) of the Akademikerbreen Group showing the $\delta^{13}C$ record (Halverson et al., 2005, 2006), along with the locations of the G1 and S1 sequence boundaries sandwiching the Bitter Springs isotope stage (Halverson et al., 2005). Also shown are the stratigraphic position of the Lower Grusdievbreen (lGfm), Upper Grusdievbreen (uGfm), and Svanbergfjellet (S4mb) paleomagnetic sampling horizons.

Springs Formation of central Australia (see Hill and Walter, 2000; Halverson et al., 2005). Two erosional surfaces bracket the Bitter Springs Stage in East Svalbard, and correspond precisely to the negative and positive shifts (7‰–8‰) in $\delta^{13}C$ that define the isotope stage. These erosion surfaces (G1 and S1) are regionally conformable (i.e., not related to block faulting during rifting or orogenesis), are overlain by lithologically identical parasequences in all sections, are the only two sequence boundaries that can be mapped along the ~150 km length of the outcrop belt, and reflect the only significant changes in relative sea level during the thermal subsidence phase of the East Svalbard platform (Halverson et al., 2005).

The lower sequence boundary (G1) displays <1 m of erosional relief on the outcrop scale (Fig. 2D). However, limestones immediately below the boundary are dolomitized, and, at least locally, paleokarst features penetrate 20 m beneath the erosion surface (Fig. 2D). G1 is overlain by a 20–30-m-thick upward-shoaling parasequence that stands out amidst a background stratigraphy of monotonous mid-to-proximal shelf limestone ribbonites. The base of this parasequence consists of silt—a rare lithology in the Akademikerbreen Group—interbedded with storm-generated intraclast breccias (Fig. 2E) and overlain by limestone ribbonites packed with formerly aragonitic seafloor cements (Fig. 2F). The substrate of the upper sequence boundary (S1) is brecciated and heavily silicified, but shows no obvious karstic relief at the outcrop scale (Fig. 2A–B). S1 is overlain by a 10–20-m-thick parasequence of black shales, shoaling upward through hummocky cross-stratified marls and into a regionally persistent *Minjaria* (sp.) stromatolite biostrome (Knoll and Swett, 1990) (Fig. 2C). The top of the parasequence is a flooding surface that marks the return to dominantly mid-to-proximal shelf limestone.

NEW MAGNETIC DATA

Paleomagnetic Results and Discussion

A suite of oriented block samples spanning the Lower Akademikerbreen Group from three continuous stratigraphic sections more than 100 km apart along the strike of the orogen was analyzed using traditional rock magnetic and paleomagnetic methods (see Appendix A). We focused our sampling on three specific stratigraphic horizons: gray limestones of the Lower Grusdievbreen Formation below G1 (lGfm), pink limestones and marls of the Upper Grusdievbreen Formation immediately above G1 (uGfm), and pink-gray limestones of the Svanbergfjellet 4 Member, ~200 m above S1 (S4mb) (Fig. 1D). We also collected samples bracketing S1 from the lower Svanbergfjellet Formation but could not accurately measure their paleomagnetic directions because the rocks were so weakly magnetized.

Prior to traditional alternating field (AF) and thermal demagnetization, a subset of samples was cooled in a LN_2 bath through the Morin transition of hematite (258 K) and the Verwey transition of magnetite (120 K). The loss of natural remanent magnetization (NRM) was always between 2%–15% (Figs. 3D, 3H, 3L, 4D, 4H, 4L, and 5D, 5H, and 5L), suggesting that no appreciable remanence is carried by multi-domain (MD) hematite or magnetite.

In all samples, a very steep magnetization component approximating the present-local magnetic field (PLF) was removed after AF demagnetization to 10 mT and heating to 150 °C (Figs. 3, 4, 5, and 6). At Raudberget (Fig. 1C), coherent thermal unblocking spectra were rare, but when a stable direction was isolated, it resembled the shallow-down, east-northeasterly direction from the Devonian of Svalbard (Jelénska and Lewandowski, 1986; Løvlie et al., 1984) and probably owed its origin to a thermochemical overprint from Silurian-Devonian felsic intrusions 2.5 km to the west. In a subset of samples from Golitsynfjellet (Fig. 1C), a moderately dipping northeasterly component (Fig. 4A–B) similar to Permian-Carboniferous directions from Svalbard (Jelénska, 1987) was removed by 350 °C. This intermediate direction is likely a magnetization overprint acquired during Carboniferous normal faulting around the Lomfjorden shear zone (Fig. 1C). At Glintbreen (Fig. 1C), the Akademikerbreen Group is intruded by thick Cretaceous dolerite sills, and some samples contain steep north-northwesterly intermediate ($INT_{IS(k)}$; Fig. 5I–J) or high-temperature overprints similar to the normal polarity mid-Cretaceous direction for Svalbard (Halvorsen, 1989).

In ~95% of samples without high-temperature Devonian or Cretaceous overprints (~85% of all of samples collected), a stable, high-temperature component decays to the origin between 350 and 600 °C, and is interpreted to represent the characteristic remanent magnetization (ChRM). Unblocking temperatures of 560–620 °C from the S4mb (Figs. 3D, 3H, and 3L), uGfm (Figs. 4D, 4H, and 4L), and rare pink limestones in the lGfm (e.g., Glintbreen; Fig. 5H) are consistent with the hypothesis that the remanent magnetization is carried by magnetite, with possible subsidiary contributions from hematite and maghemite. Lower unblocking temperatures of 400–500 °C (Figs. 5D and 5L) for the lGfm black limestones are consistent with the idea that titanomagnetite is the principal remanence carrier (Dunlop and Özdemir, 1997).

The paleomagnetic directions derived through principal component analysis (Kirschvink, 1980) of thermal unblocking spectra are summarized in Figure 6, and section mean statistics are reported in Table 1. The majority of thermal unblocking spectra show linear decay to the origin, and high-temperature components are fit by lines forced through the origin (Figs. 3A–C, 3E–G, 3I–K, 4A–C, 4E–G, 5A–C, 5E–G, and 5I–K). However, 45% of uGfm samples and 25% of lGfm samples display arcuate thermal unblocking spectra, suggesting the presence of overlapping magnetic components. In such cases, high-temperature components were delineated by fitting great circles to thermal unblocking spectra (e.g., Fig. 4E–G) and making use of arc constraints (McFadden and McElhinny, 1988) to narrow the range of possible directions. Great circle fits were given half the weight of line fits during computation of sample mean and section mean statistics.

The lGfm, uGfm, and S4mb ChRMs are derived from 10 to 100 m of stratigraphic section (>10^4 yr) and show moderate standard deviation about their means, suggesting that the ChRMs reflect adequate time-averaging of geomagnetic secular variation. Because the lGfm, uGfm, and S4fm directions are derived from carbonates that experienced early cementation, ChRMs are unlikely to have experienced significant compaction-induced inclination shallowing during burial, which predominantly affects shales and coarser, clay-bearing detrital rocks (e.g., Anson and Kodama, 1987; Tauxe and Kent, 1984; Jackson et al., 1991; Kodama and Sun, 1992; Tan and Kodama, 1998; Gilder et al., 2003; Tan et al., 2003; Kim and Kodama, 2004), and should record faithfully the true inclination of the ancient geomagnetic field.

Reversed magnetic polarities are preserved in 16 of 111 uGfm samples (14%) and 5 of 57 (9%) lGfm samples (Figs. 6F, 6G, and 7). The 95% confidence circles for mean normal and mean reversed directions overlap for both the uGfm and lGfm. Consistent normal and reversed polarity intervals are recognized within the three uGfm stratigraphic sections separated by >100 km (Fig. 7). Nevertheless, McFadden and McElhinny's (1990) reversal tests were inconclusive for both uGfm and lGfm because the collection of reverse polarity samples was too small.

The uppermost 0.5–1.5 m of the lGfm is dolomitized directly beneath the G1 sequence boundary (Fig. 7). Compared to underlying limestones, these diagenetically altered dolostones have 2–5× weaker NRMs and show an ~20° eastward offset of their ChRMs. It is possible that the lGfm dolomites record a chemical remagnetization during G1 karstification. However, only five specimens were collected from this horizon, so it was not possible to determine a reliable paleomagnetic direction.

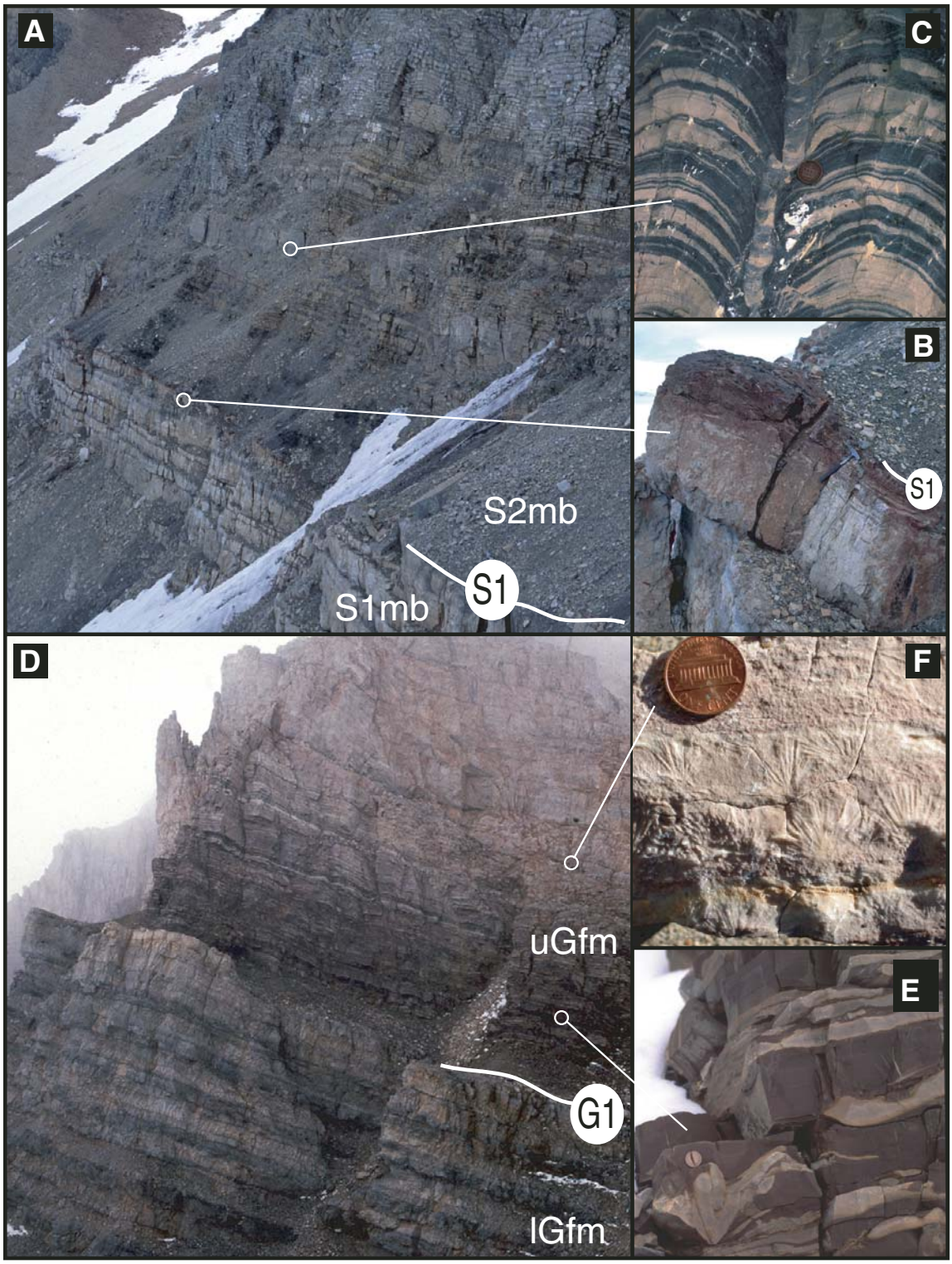

Figure 2. Field photographs of the Grusdievbreen and Svanbergfjellet Formations. (A) S1 sequence boundary (white line) separating Svanbergfjellet 1 (S1mb) and Svanbergfjellet 2 (S2mb) members at Svanbergfjellet (Fig. 1C). Despite brecciation, silicification, and ferruginization of the sequence boundary (B), there is no evidence of erosional relief on the outcrop scale (in B, hammer is 33 cm long). (C) *Minjaria* sp. stromatolites form a distinctive biostrome 10–15 m above the S1 boundary throughout northeast Svalbard (Knoll and Swett, 1990). (D) G1 sequence boundary (white line) separating the Upper (uGfm) and Lower (lGfm) Members of the Grusdievbreen Formation at North Golitsynfjellet (Fig. 1C). Note the ~2 m of karstic relief on the dolomitized (beige) G1 contact and the sharp change in parasequence lithology above the boundary. A green silt fills in the erosional relief on G1, and is overlain by edgewise limestone breccias (E) and aragonite pseudomorphs ("crystal fans") that form a continuous seafloor cement (F). Pennies in C, E, and F are 1.9 cm in diameter.

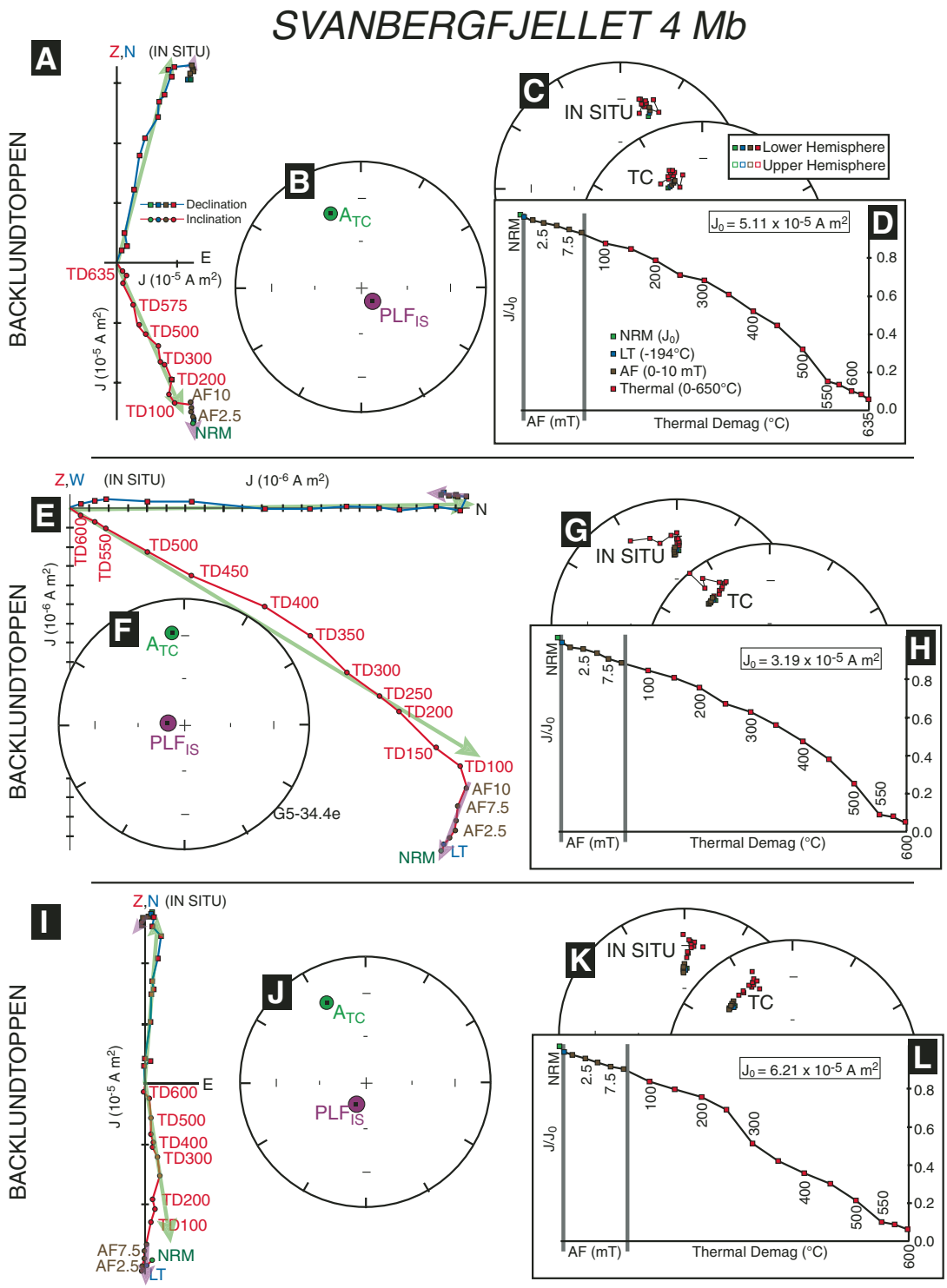

Figure 3. Representative vector component diagrams (Zijderveld, 1967) (A, E, and I), least-squares fits (B, F, and J), equal-area projections (C, G, and K), and magnetic intensity (J/J_0) plots (D, H, and L) showing demagnetization behavior for the Svanbergfjellet 4 Member (S4mb). In the Zijderveld plots (always in situ coordinates), the primary, high-temperature component that decays to the origin is traced with a green arrow, and the present local field (PLF) overprint is traced with a purple arrow. Least-squares fits of these components, with error ovals representing circular maximum angular deviation (MAD) angles from the principal component analysis (plotted using the routines of Cogné [2003]), are summarized in an adjacent equal-area projection (B, F, and J), and are labeled A_{TC} and PLF_{IS}, respectively, where TC refers to tilt-corrected and IS refers to in situ coordinates. In all plots, green-filled shapes are natural remanent magnetization (NRM) directions, blue-filled shapes are the low-temperature step, brown-filled shapes reflect alternating field (AF) demagnetization steps, and red-filled shapes reflect thermal demagnetization. In the Zijderveld plots (A, E, and I), squares/circles represent declination/inclination, while in the equal-area nets (C, G, and K), color-filled/color-rimmed squares represent lower/upper-hemisphere directions.

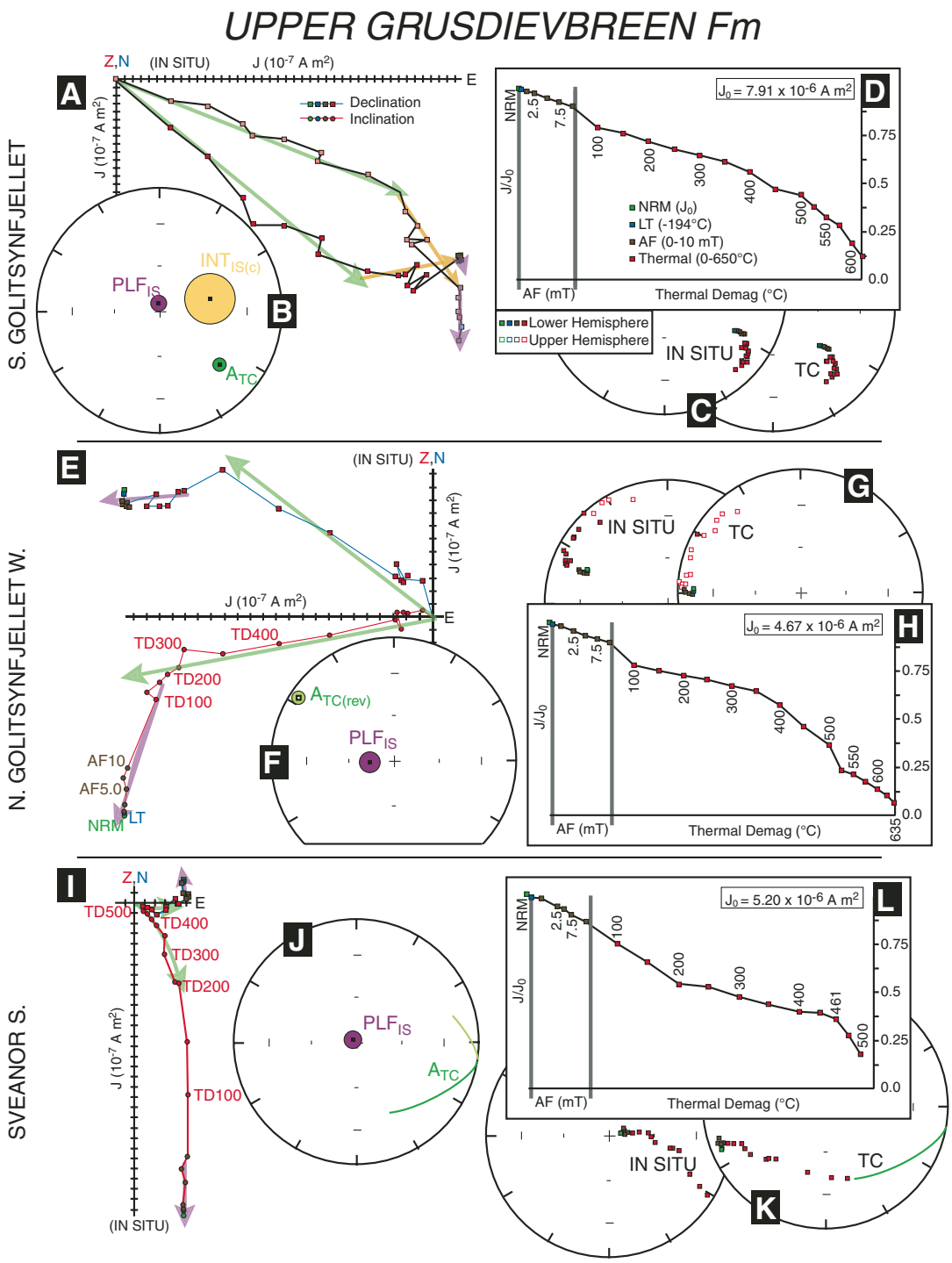

Figure 4. Representative vector component diagrams (Zijderveld, 1967) (A, E, and I), least-squares fits (B, F, and J), equal-area projections (C, G, and K) and magnetic intensity (J/J_0) plots (D, H, and L) showing demagnetization behavior for the Upper Grusdievbreen Formation (uGfm). In the Zijderveld plots (always in situ coordinates), the primary, high-temperature component that decays to the origin is traced with a green arrow, intermediate directions, when present, are traced with a yellow arrow, and the present local field (PLF) overprint is traced with a purple arrow. When thermal unblocking spectra are arcuate, rather than linear, a great circle is fit to the data instead of a line (I–K). Least-squares fits of these components, with error ovals representing circular maximum angular deviation (MAD) angles from the principal component analysis (plotted using the routines of Cogné [2003] and Jones and Tetreault [2004]), are summarized in an adjacent equal-area projection (B, F, and J), and are labeled A_{TC}, $INT_{IS(c)}$, and PLF_{IS}, respectively, where TC refers to tilt-corrected and IS refers to in situ coordinates. In all plots, green-filled shapes are natural remanent magnetization (NRM) directions, blue-filled shapes are the low-temperature step, brown-filled shapes reflect alternating field (AF) demagnetization steps, and red-filled shapes reflect thermal demagnetization. In the Zijderveld plots (A, E, and I), squares/circles represent declination/inclination, while in the equal-area nets (C, G, and K), color-filled/color-rimmed squares represent lower/upper-hemisphere directions.

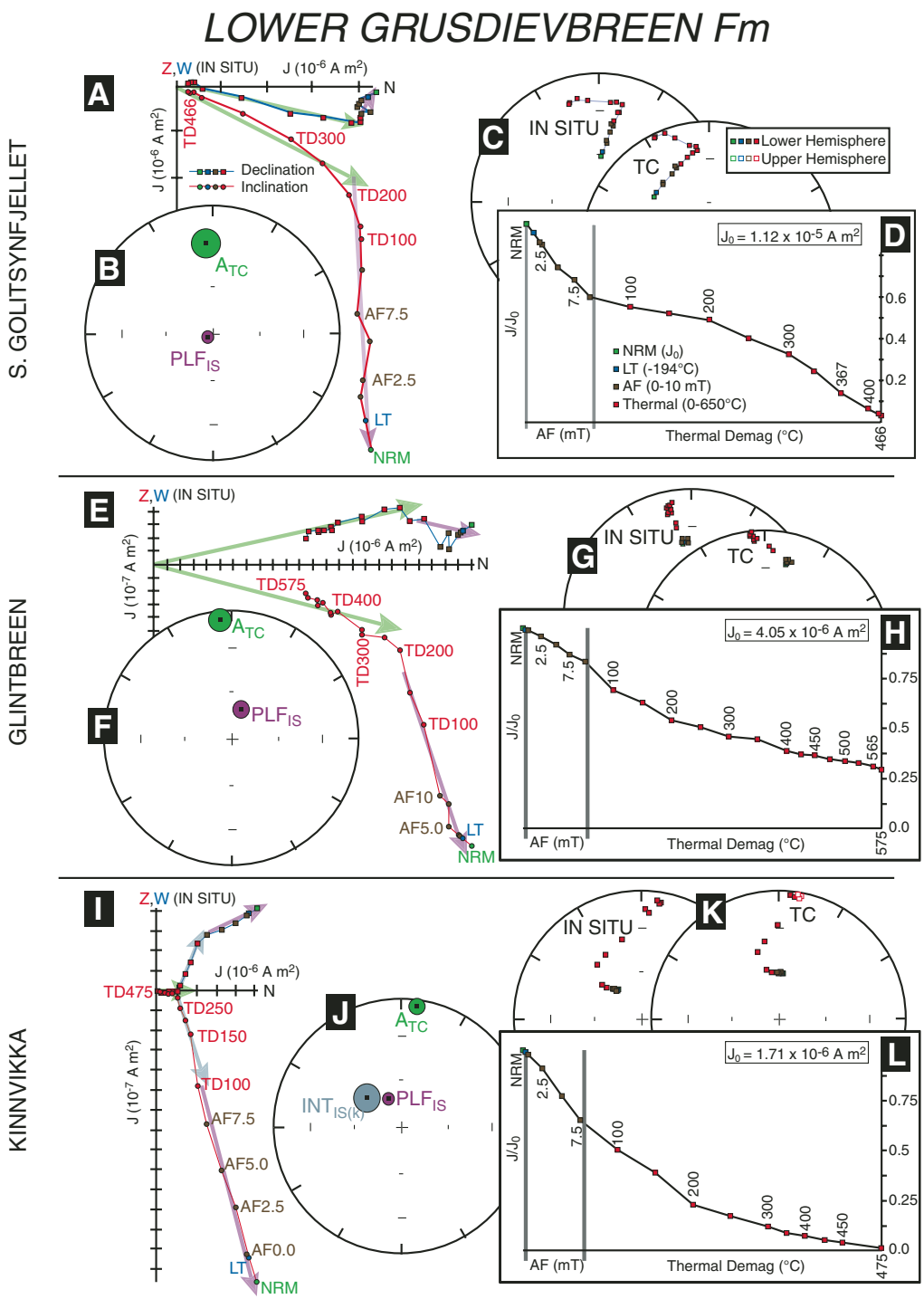

Figure 5. Representative vector component diagrams (Zijderveld, 1967) (A, E, and I), least-squares fits (B, F, and J), equal-area projections (C, G, and K) and magnetic intensity (J/J_0) plots (D, H, and L) showing demagnetization behavior for the Lower Grusdievbreen Formation (lGfm). In the Zijderveld plots (always in situ coordinates), the primary, high-temperature component that decays to the origin is traced with a green arrow, intermediate directions, when present, are traced with a gray arrow, and the present local field (PLF) overprint is traced with a purple arrow. Least-squares fits of these components, with error ovals representing circular maximum angular deviation (MAD) angles from the principal component analysis (plotted using the routines of Cogné [2003]), are summarized in an adjacent equal-area projection (B, F, and J), and are labeled A_{TC}, $INT_{IS(k)}$, and PLF_{IS}, respectively, where TC refers to tilt-corrected and IS refers to in situ coordinates. In all plots, green-filled shapes are natural remanent magnetization (NRM) directions, blue-filled shapes are the low-temperature step, brown-filled shapes reflect alternating field (AF) demagnetization steps, and red-filled shapes reflect thermal demagnetization. In the Zijderveld plots (A, E, and I), squares/circles represent declination/inclination, while in the equal-area nets (C, G, and K), color-filled/color-rimmed squares represent lower/upper-hemisphere directions.

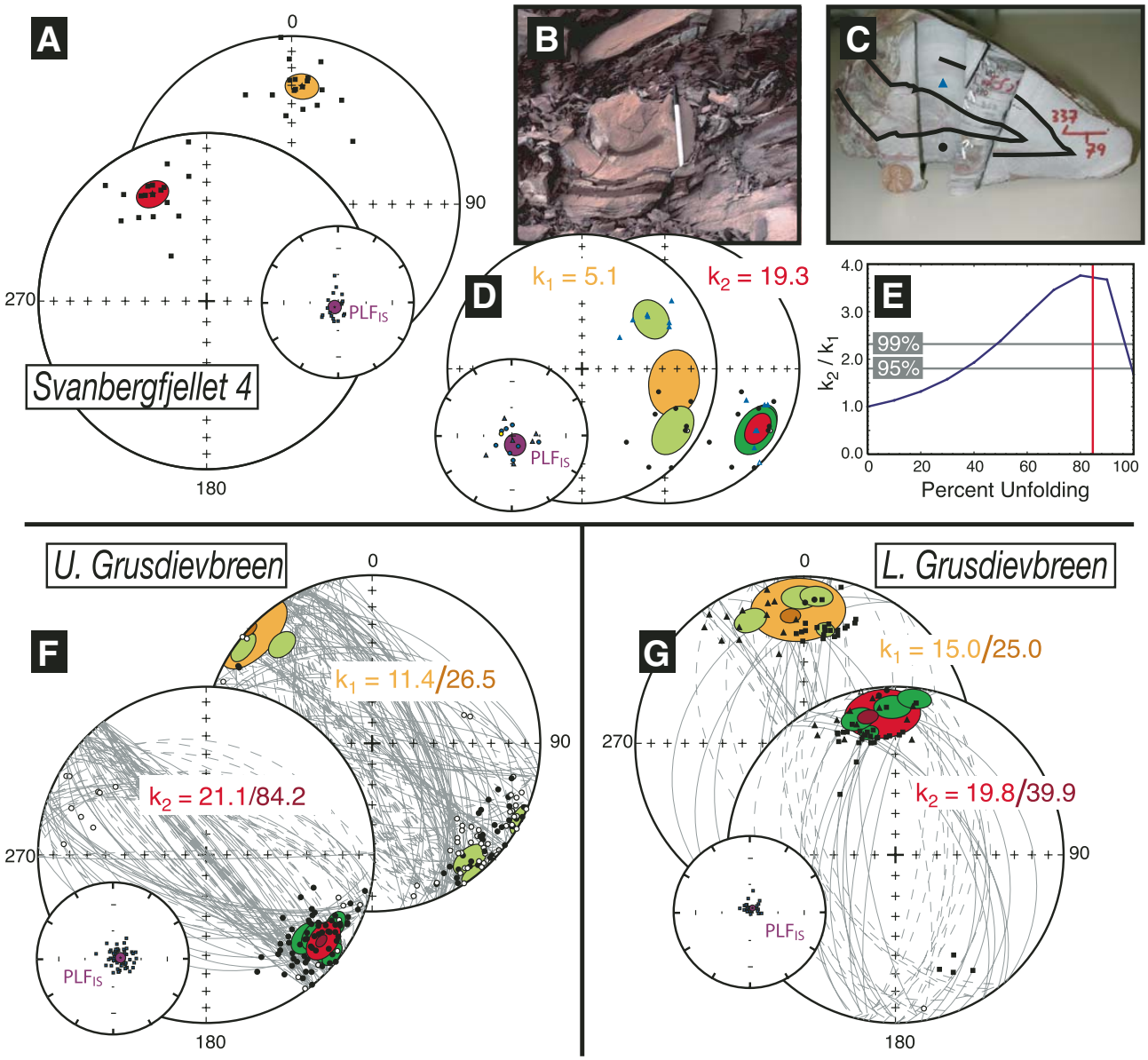

Figure 6. Tests for the presence of prefolding or synfolding magnetization. Equal-area nets show in situ (orange) and tilt-corrected (red) Fisher distributions of the characteristic remanent magnetization (ChRM) direction and in situ distribution of the present-local field (PLF) overprint (purple) for the Lower Grusdievbreen (lGfm) (G), Upper Grusdievbreen (uGfm) (F), and Svanbergfjellet (S4mb) (A). Filled/open circles are lower/upper-hemisphere least-squares line fits to demagnetization curves. Gray arcs are great circle fits to demagnetization curves with overlapping magnetic components. Where multiple stratigraphic sections are present, as in (F) and (G), individual section-mean Fisher statistics are plotted as light green (in situ) and dark green (tilt-corrected) ellipses, while the averages of section-mean directions are plotted as dark orange (in situ) and dark red (tilt-corrected) ellipses. Values k_1 and k_2 are in situ and tilt-corrected Fisher (Fisher, 1953) concentration parameters measuring the dispersion in individual paleomagnetic data (light orange and light red) and site-mean paleomagnetic data (dark orange and dark red). S4mb contains numerous disturbed beds of pink limestone and red marl with detached synsedimentary folds (B) and erosional truncations (left of the pen cap in B). Paleomagnetic directions from the upper limb (blue triangles) and lower limb (black circles) of the fold pictured in C are plotted on the equal-area net in D. The PLF overprint direction fails the fold test, while the primary magnetic component passes the synsedimentary fold test at the 99% confidence level (E). (E) Shows that k_2/k_1 is maximized at 86% unfolding and that the S4mb ChRM was likely acquired prior to, or at the onset of slump folding, and thus dates from the time of sedimentation. (Note: the demagnetization behavior of the ChRM from A and D is identical, and the two directions are considered to reflect the same paleomagnetic component. The difference in absolute direction of the ChRM in D with respect to the ChRM in A is just another reflection of the observation that the ChRM was acquired prior to disruption and folding.) Both the uGfm (F) and lGfm (G) directions were derived from multiple stratigraphic sections separated by >100 km. Although paleomagnetic directions are subparallel to the NNW-trending Caledonian fold axes, k_2/k_1 is maximized at 100% unfolding, and both uGfm and lGfm pass the McElhinny (1964) fold test at greater than the 92% confidence level.

TABLE 1. PALEOMAGNETIC DATA FROM EAST SVALBARD

Formation/ section	Location N00°00′	Location E00°00′	Magnetic declination (°E)	n/N	In situ coordinates D_m (°E)	I_m (°N)	k_1	α_{95} (°)	Tilt-corrected coordinates D_m (°E)	I_m (°N)	k_2	α_{95} (°)	λ (°N)	ϕ (°E)	*dp* (°)	*dm* (°)	Plat (°)
Svanbergfjellet 4 Mb																	
Backlundtoppen	N78°30′	E18°00′	(4°)	18/19	5.0	30.3	25.0	7.1	333.2	29.4	25.2	7.0	25.9	226.8	4.3	7.7	$15.7^{+20.2}_{-11.6}$
U. Grusdievbreen Fm																	
S. Golitsynfjellet	N78°42′	E18°18′	(4°)	38/38	142.3	1.7	19.6	4.3	128.4	5.3	16.2	4.7	–4.4	69.7	2.4	4.7	$-2.7^{+5.0}_{-0.3}$
N. Golitsynfjellet E	N78°45′	E18°18′	(4°)	24/24	117.3	0.9	35.7	4.8	118.6	14.0	28.1	5.5	1.7	78.6	2.9	5.6	$-7.1^{+7.8}_{-1.7}$
N. Golitsynfjellet W	N78°45′	E18°18′	(4°)	21/22	126.8	–4.7	30.4	5.9	127.6	9.3	29.0	6.0	–2.2	70.2	3.1	6.1	$-4.7^{+10.0}_{-4.3}$
Sveanor S	N79°56′	E18°31′	(6°)	20/22	139.9	10.4	9.0	10.9	130.1	23.7	21.7	7.2	5.7	69.7	4.1	7.7	$-12.4^{+16.7}_{-8.4}$
Sveanor N	N79°52′	E18°30′	(6°)	4/5	137.6	–21.5	223.7	6.2	127.1	20.9	223.7	6.2	4.6	72.8	3.4	6.5	$-10.8^{+14.4}_{-7.5}$
TOTAL(samples)				107/111	133.1	–1.1	11.4	3.5	126.9	15.9	21.1	2.7	1.6	71.9	1.4	2.8	$-8.1^{+9.6}_{-6.7}$
TOTAL(sections)				5/5	132.7	–2.6	26.5	15.1	126.3	14.7	84.2	8.4	1.1	72.6	4.4	8.6	$-7.5^{+12.0}_{-3.2}$
L. Grusdievbreen Fm																	
S. Golitsynfjellet	N78°42′	E18°18′	(4°)	24/26	10.8	30.5	57.3	3.9	347.5	26.5	57.3	3.9	25.0	211.4	2.3	4.2	$14.0^{+16.3}_{-11.8}$
N. Golitsynfjellet	N78°45′	E18°18′	(4°)	6/7	358.8	12.7	66.7	7.0	358.5	12.9	65.2	7.1	17.7	199.9	3.7	7.2	$6.5^{+10.3}_{-2.9}$
Glintbreen	N79°25′	E17°53′	(4°)	18/19	337.1	20.2	27.6	6.2	344.1	17.1	24.3	6.6	19.1	215.0	3.5	6.8	$8.7^{+12.4}_{-5.3}$
Kinnvikka	N80°05′	E18°20′	(3°)	5/5	5.1	11.7	113.1	6.3	6.6	7.2	116.0	6.2	13.7	194.2	3.1	6.2	$3.6^{+6.8}_{-0.5}$
TOTAL(samples)				53/57	354.4	23.4	15.0	4.8	348.3	17.3	19.8	4.1	19.6	211.3	2.2	4.2	$8.9^{+11.1}_{-6.7}$
TOTAL(sections)				4/4	357.9	19.2	25.0	18.8	354.4	16.1	39.9	14.7	19.6	204.9	7.9	15.2	$8.9^{+17.4}_{-1.3}$

Notes: n—number of stratigraphic horizons or samples used in this study; N—total number of stratigraphic horizons or samples collected, where great-circle fits are weighted as 1/2 and line fits are weighted as 1; D_m and I_m—mean declination and inclination of *N* stratigraphic horizons or samples; *k*—Fisher's (1953) precision parameter; α_{95}—radius of confidence circle for the mean direction; λ and ϕ—latitude and longitude of paleopole for mean direction in present-day East Svalbard coordinates; *dp* and *dm*—semiminor and semimajor axes of 95% polar error ellipse; Plat—paleolatitude.

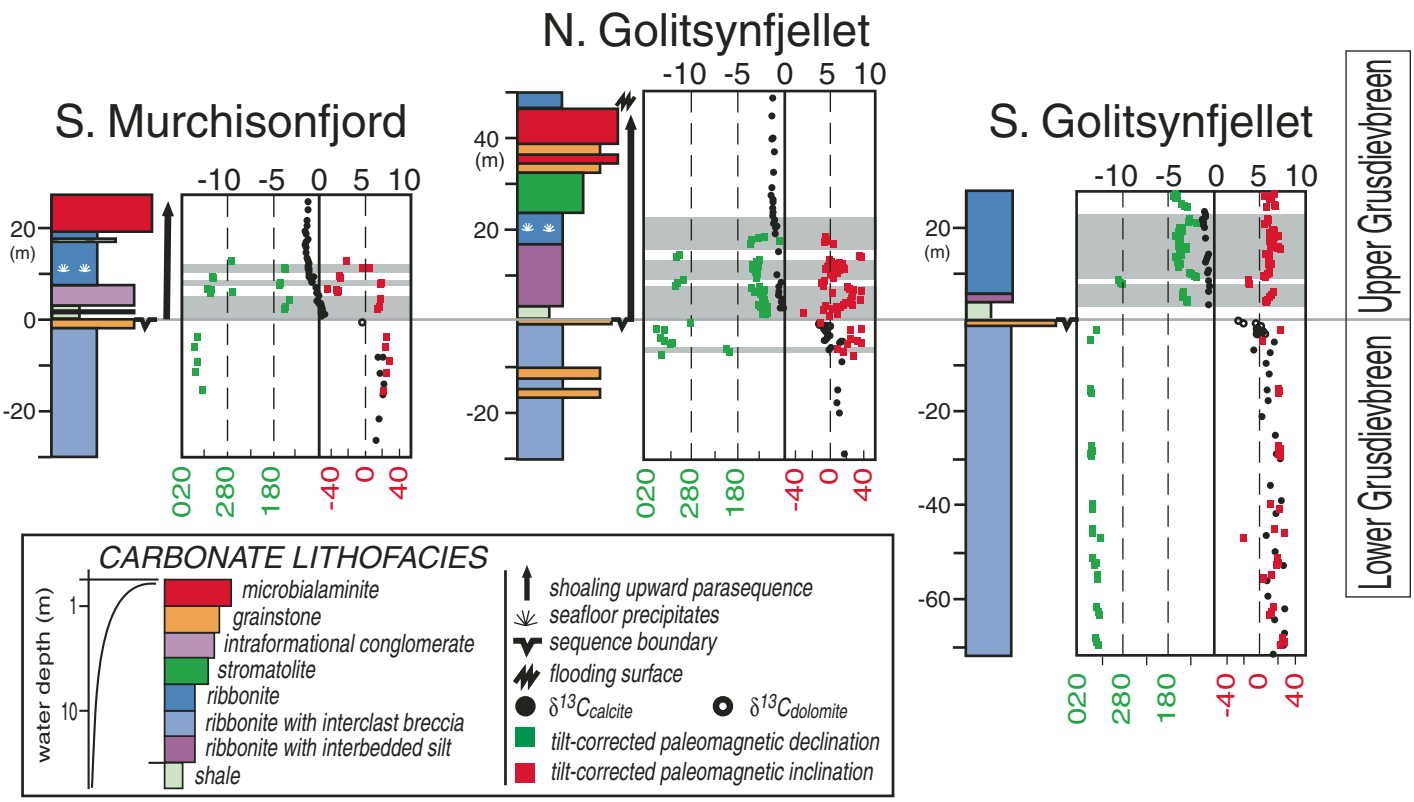

Figure 7. Paleomagnetic and carbon-isotope stratigraphy across the G1 sequence boundary. Carbon isotope data for calcite/dolomite are plotted with solid/open black circles, while tilt-corrected paleomagnetic declination and inclination are plotted with solid green and red squares, respectively. White and gray areas correspond to opposite magnetic polarities. Stratigraphic height is set to 0 meters at the GI sequence boundary. Carbonate lithofacies are color coded, and wider boxes reflect depositional environments in shallower water. Seafloor precipitates are thought to be calcite pseudomorphs after aragonite.

Age of Magnetization

A paleomagnetic fold test compares ChRM directions for in situ (geographic) coordinates to ChRMs rotated to a tilt-corrected or "unfolded" coordinate system. If a ChRM was acquired prior to folding, in situ paleomagnetic directions should be more dispersed than bedding-tilt-corrected directions.

The S4mb ChRM was isolated from a single stratigraphic section with uniform tilt-correction (Fig. 6A), so a tectonic fold test was not possible. However, the unit contains numerous disturbed beds of pink limestone and red marl with detached synsedimentary folds and erosional truncations (Fig. 6B–C). In the fold pictured in Figure 6C, the PLF overprint direction fails the fold test, while the primary magnetic component passes the synsedimentary fold test at the 99% confidence level (Fig. 6D). The ratio of tilt-corrected and in situ Fisher (1953) precision parameters k_2/k_1 is maximized at 86% unfolding (Fig. 6E), indicating that the Svanbergfjellet 4 Mb ChRM was acquired prior to, or at the onset of slump folding. Therefore, the S4mb ChRM was acquired during sedimentation or earliest diagenesis.

The uGfm and lGfm do not contain synsedimentary folds large enough for analysis by conventional paleomagnetic techniques. However, Akademikerbreen Group strata of East Svalbard are deformed by NNW-SSE–trending folds of Caledonian (Silurian-Devonian) age. After 100% tilt correction, both lGfm and uGfm directions show decreases in dispersion (i.e., $k_1 < k_2$; Fig. 6F–G). For lGfm, the rather lenient McElhinny (McElhinny, 1964) fold test is positive at the 92% confidence level when evaluating sample statistics and at the 70% level when considering section mean statistics. For uGfm, the McElhinny (McElhinny, 1964) fold test is positive at the 99% confidence level when evaluating sample statistics and at the 93% confidence level for section mean statistics. When using the more stringent fold test of McFadden and Jones (McFadden and Jones, 1981; McFadden, 1998), the ratio of dispersion of group means to within group dispersion does decrease by a factor of two upon 100% unfolding; however, the fold test is inconclusive. The McFadden and Jones fold test likely is inconclusive for two reasons: (1) our sites are not adequately distributed around the limbs and hinge zone of the fold, and (2) the uGfm, and particularly lGfm, ChRMs are subparallel to the strike of regional folds, so tilt correction induces only slight changes to the paleomagnetic directions. Nevertheless, the visible decrease in the dispersion of both sample and site mean directions after tilt correction suggests that the ChRM directions in both the lGfm and uGfm were acquired prior to Silurian-Devonian folding.

The lGfm, uGfm, and S4mb ChRMs are unlike any regional overprints known from the Devonian (Jelénska and Lewandowski, 1986; Løvlie et al., 1984), Carboniferous-Permian (Jelénska and Vincenz, 1987; Watts, 1985), Permian-Triassic (Nawrocki, 1999), and Jurassic-Cretaceous (Halvorsen, 1989; Spall, 1968). No thermal or deformation events have been recognized in East Svalbard between Middle Neoproterozoic and Silurian time. In fact, the only major stratigraphic break recorded during this interval is an Ediacaran to late Early Cambrian (ca. 580–520 Ma) hiatus. Unfortunately, the hypothesis that both uGfm and lGfm are Ediacaran-Cambrian overprints cannot be tested directly because global apparent polar wander paths are highly contentious during this interval (e.g., Kirschvink et al., 1997; Torsvik et al., 1998; Evans et al., 1998; Meert, 1999; Pisarevsky et al., 2000; Meert et al., 2001; Evans, 2003), and Laurentia's absolute paleogeographic position is unknown. Nevertheless, the combination of positive tectonic fold tests, evidence for a reversing paleomagnetic field, and the uniqueness of the three paleomagnetic directions suggests that, like the S4fm ChRM, the uGfm and lGfm ChRMs were acquired during sedimentation or earliest diagenesis.

Rock Magnetic Results and Discussion

The many examples of carbonate remagnetization in North America emphasize the need to be careful when interpreting the origin of magnetite in platform limestones (e.g., McCabe and Elmore, 1989; Van der Voo, 1989). In Lower Paleozoic carbonates of the midcontinental United States, large fractions of very fine-grained superparamagnetic (SP) magnetite (0.30 nm) and coarse-grained spheroidal or botryoidal multidomain (MD) magnetite (and 300 nm) appear to have precipitated authigenically under the influence of migrating fluids (Jackson, 1990; Jackson et al., 1992). The Pennsylvanian-Permian age of remagnetization has led numerous authors to suggest that tectonic fluids originating from orogenic activity along the margins of North America were the cause (McCabe et al., 1983, 1989; Oliver, 1986; Miller and Kent, 1988).

On the other hand, not all magnetite in ancient carbonate rocks is secondary, since both wind-blown dust and magnetotactic bacteria may be important sources of magnetite. Modern Bahamian carbonates contain abundant single-domain (SD) magnetite (~30–80 nm) of possible biogenic origin (e.g., Moskowitz et al., 1988, 1993; Stolz et al., 1986; Vali and Kirschvink, 1989; Weiss et al., 2004) that faithfully records Earth's present geomagnetic field (Maloof et al., 2005). Furthermore, Cenozoic carbonates from the Bahamas preserve primary magnetostratigraphy despite extensive bioturbation and variable degrees of burial diagenesis and dolomitization (McNeill and Kirschvink, 1993; McNeill, 1997).

A basic understanding of rock magnetic properties in the Akademikerbreen Group strata will help us evaluate the possibility that they were remagnetized during a hitherto unrecognized chemical event in latest Neoproterozoic or Cambrian times. Five samples from the lGfm, six samples from the uGfm, and two samples from the S4mb were subjected to low-temperature cycling and hysteresis experiments, as well as electron microscopy. Rock magnetic methods are described in Appendix A.

The uGfm and S4mb samples behaved similarly during rock magnetic experiments (Figs. 8A and 8C). We suggest that magnetite is the dominant carrier of magnetic remanence

Figure 8. Representative low-temperature cycling (A, C, E) and hysteresis (B, D, F) experiments on Svanbergfjellet (S4mb) (A, B), Upper Grusdievbreen (uGfm) (C, D), and Lower Grusdievbreen (lGfm) (E, F) samples. In the low-temperature cycling plots (A, C, E), blue curves are cooling trajectories, red curves are warming trajectories, and black curves are the first derivatives of the cooling trajectory. In the low-temperature cycling experiments on S4mb and uGfm, remanence recovery ratios of ≥91% and Verwey transitions at 120 K suggest that single-domain (SD) magnetite is the principal carrier of remanence. In lGfm, an isotropic point at 60 K and remanence recovery ratios of ~85% suggest that SD-PSD titanomagnetite is the principal remanence carrier (PSD is pseudo-single domain). Remanence recovery ratios are defined as the natural remanent magnetization (NRM) (at 300 K) measured prior to low-temperature cycling divided by the NRM (at 300 K) measured after low-temperature cycling. Hysteresis experiments, summarized in Figure 9, are consistent with results from low-temperature cycling. Inset plots in B, D, and F show the saturation magnetizations attained during the full hysteresis experiment (after correction for high-field paramagnetic/diamagnetic behavior).

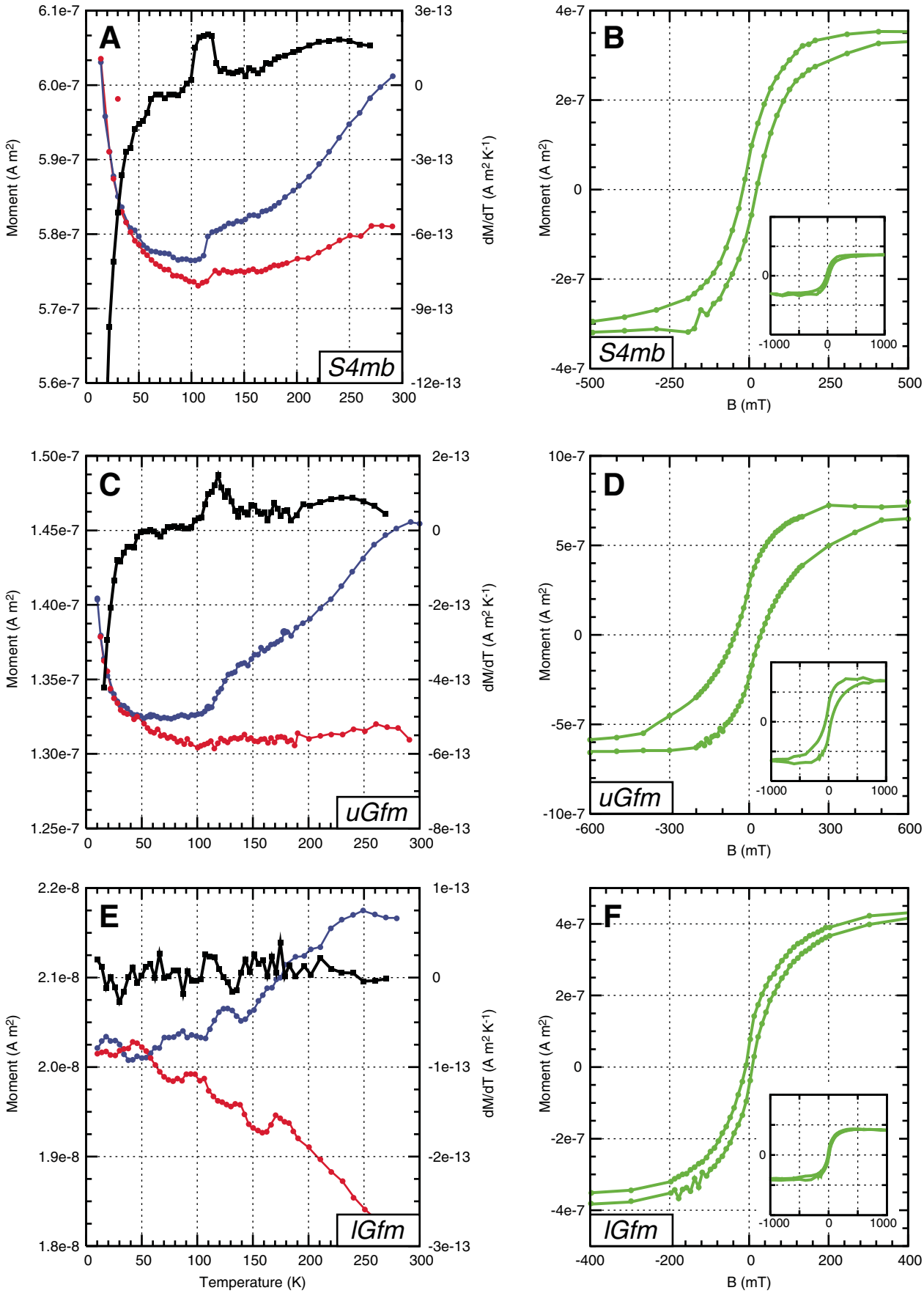

because (1) the steep Verwey transition at 120 K indicates the presence of a population of fairly stoichiometric Fe_3O_4 (Figs. 8A and 8C); and (2) the unblocking temperature ranges between 560 and 600 °C (Figs. 3D, 3H, 3L, 4D, 4H, and 4L), similar to the 580 °C Curie point for pure magnetite. The fact that the cooling curves do not overlap the warming curves until ~50 K (Figs. 8A and 8C) suggests that a subpopulation of grains, such as titanomagnetite (~$Fe_{2.8}Ti_{0.2}O_4$), may coexist with the more stoichiometric magnetite in these samples (see the following discussion of lGfm). Also, slightly elevated unblocking temperatures (Figs. 3D, 3H, 3L, 4D, and 4H) and coercivities (Figs. 8B and 8D) may point to a subordinate population of maghemite.

We suggest that the magnetites in uGfm and S4mb specimens are mostly SD and pseudo-single domain (PSD, ~70–200 nm) because (1) remanence recoveries following low-temperature cycling of 91%–96% (measured at 300 K; Figs. 8A and 8C) imply that these rocks are dominated by grains with diameters between 30 and 200 nm (Dunlop and Özdemir, 1997; Halgedahl and Jarrard, 1995); (2) hysteresis data (Figs. 8B and 8D) summarized on an SC plot (Fig. 9) indicate the prevalence of SD and PSD magnetite; and (3) no magnetite grains were large enough to image confidently with the Electron Probe X-ray Microanalyzer (EMPA). The steep remanence increase between 30 K and 10 K (Figs. 8A and 8C), the "wasp-waisted" shape of the hysteresis loops (Figs. 8B and 8D), and the high coercive field (Bc) values suggest the additional presence of a population of SP grains.

The lGfm behaves differently from the uGfm and S4mb. We suggest that the lGfm remanence is carried predominantly by titanomagnetite because: (1) any Verwey transition appears to be severely depressed, but the possible presence of an isotropic point at ~60 K suggests a population of grains dominated by compositions between $Fe_{2.85}Ti_{0.15}O_4$ and $Fe_{2.67}Ti_{0.33}O_4$ (Moskowitz et al., 1998); (2) unblocking temperatures of 400–500°C suggest similar titanomagnetite compositions (Özdemir and Dunlop, 2003); and (3) the presence of a broad peak in the cooling curve at 250 K is indicative of titanomagnetite (Özdemir and Dunlop, 2003).

We suggest that the titanomagnetite is predominantly PSD and SD because: (1) the lack of any remanence increases between 30 K and 10 K suggests a dearth of superparamagnetic grains; (2) the shape of the hysteresis curve (Fig. 8F) and the SC plot summary (Fig. 9) are indicative of PSD grains (although the fields on the SC plot have not been calibrated specifically for titanomagnetite); (3) no MD magnetic grains were visible with the EMPA; and (4) the 85%–90% remanence recovery (measured at 300 K; Fig. 8E) implies that these rocks are dominated by SD and PSD grains. Note, however, that point 4 is inconclusive because MD titanomagnetites have been found to show more effective remanence recovery than similarly sized magnetite grains (Özdemir and Dunlop, 2003). Nevertheless, the very small overall remanence loss (<10% during cooling (Figs. 5D, 5H, and 5L) suggests that MD magnetite cannot make up a large fraction of the magnetic grains in the rock.

We did not detect populations of primary or authigenic MD magnetite in lGfm, uGfm, and S4mb in rock magnetic experiments or with optical and scanning electron microscopy. Although both the uGfm and S4mb have fractions of SP magnetite that could be authigenic, the S4mb passes a synsedimentary fold test and therefore has a primary magnetic remanence that is not affected by secondary growth of SP or SD grains. We cannot rule out the possibility that SD grains in the lGfm and/or uGfm are authigenic and latest Neoproterozoic or Cambrian in age. However, the combination of magnetostratigraphic reproducibility and the lack of nearby 580–520 Ma orogenesis argues for a detrital or earliest diagenetic origin for the ChRM in the lGfm, uGfm, and S4mb.

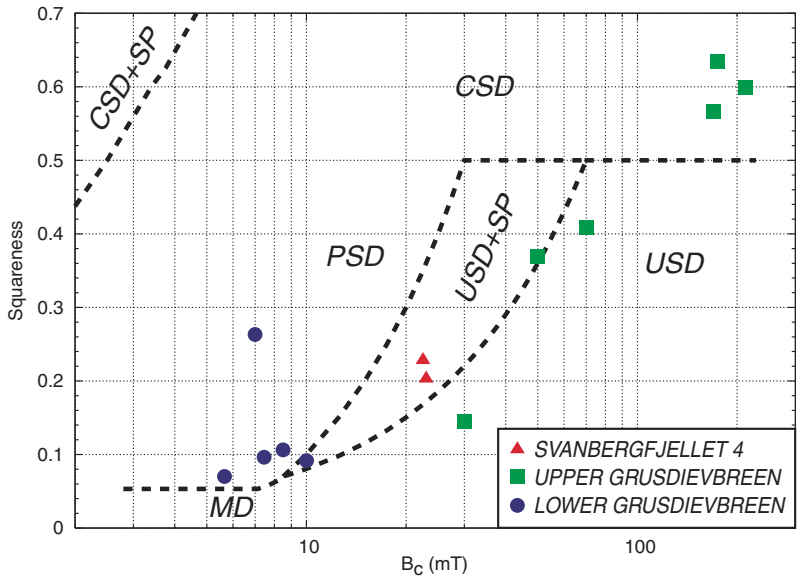

Figure 9. Summary plot of squareness (M_r/M_s) versus coercive field (B_c) for Svanbergfjellet (S4mb), Upper Grusdievbreen (uGfm), and Lower Grusdievbreen (lGfm) samples. Dashed black lines delineate approximate boundaries for magnetite size fractions, where CSD is hypothetical cubic single domain, SP is superparamagnetic, USD is uniaxial single domain, PSD is pseudo-single domain, and MD is multidomain (Tauxe et al., 2002).

TIME SCALE

The Veteranen Group (Fig. 1D) is known to be younger than 940 Ma by U-Pb ages from igneous zircons in basement granites of Nordaustlandet (Gee et al., 1995; Johannson et al., 2001). Climatic deterioration and possibly glacioeustatic third-order sea-level variability near the top of the Akademikerbreen Group has been related to the growth of Sturtian ice sheets (Halverson et al., 2005, 2004). A U-Pb zircon date of 746 ± 2 Ma from 700 m below the Sturtian diamictite in northern Namibia provides a useful maximum age constraint for the glacial event (Hoffman et al., 1996). However, a minimum age for the onset of Sturtian glaciation is more elusive. Sturtian glacial deposits in Oman and Idaho (USA) contain volcanic units that have been U-Pb zircon dated to 712 ± 2 Ma (Bowring et al., 2003; Brasier et al., 2000) and 709 ± 5 Ma (Fanning and Link, 2004), respectively. For the purpose of approximating the age of the top of the Akademikerbreen Group and allowing for the chance that Sturtian glaciation is not globally synchronous, we consider scenarios where the onset of Sturtian glaciation took place at either ca. 740 Ma or 710 Ma.

A simple McKenzie-type (LePichon and Sibuet, 1981; McKenzie, 1978) thermal subsidence model (Appendix B), assuming instantaneous stretching during the Veteranen rift phase, predicts that the Akademikerbreen Group was deposited in ~90 m.y. (Fig. 10). Tying one end of the thermal subsidence trajectory to the onset of Sturtian glaciation suggests that Akademikerbreen Group sedimentation began ca. 820 Ma

and that the Bitter Springs Stage spanned the interval ca. 803–792 Ma (Fig. 10). Allowing initial crustal and lithospheric thicknesses to vary between 30 and 40 km and 100 and 125 km, respectively, does not change the result significantly. This time scale is consistent with the correlation of the Upper Grusdievbreen and Lower Svanbergfjellet Formations (East Svalbard) with the Loves Creek Member of the Bitter Springs Formation (Amadeus Basin, South Australia) and the Curdimurka Subgroup (Southern Flinders Ranges, South Australia) (Halverson et al., 2005; Hill et al., 2000b; Preiss, 2000). The ca. 825 Ma Wooltana volcanics (correlated with the 827 ± 6 Ma Gairdner Dykes (Preiss, 2000) underlie the Curdimurka Subgroup and provide a maximum age for the Bitter Springs Stage. The Lower Curdimurka is within the base of the Bitter Springs Stage and contains the Rook Tuff, which has a U-Pb zircon age of 802 ± 10 Ma (Fanning et al., 1986). The top of the Curdimurka is likely older than the 777 ± 7 Ma U-Pb zircon date for the Boucat volcanics correlated with the overlying Burra Group (Preiss, 2000).

Admittedly, the subsidence model in Appendix B is oversimplified, and some amount of thermal subsidence must have occurred during the rifting phase. In the extreme case where 50% of the total thermal subsidence occurred during prolonged rifting, the Bitter Springs Stage is shifted back to ca. 850 Ma and lasts for ~20 m.y. This scenario is not consistent with the correlation to Australian chemostratigraphy and geochronology described already. However, even given stratigraphic correlations, thermal subsidence histories, and initial crustal and lithospheric thicknesses radically different than those preferred here, the duration of the Bitter Springs Stage in Svalbard was likely <20 m.y.

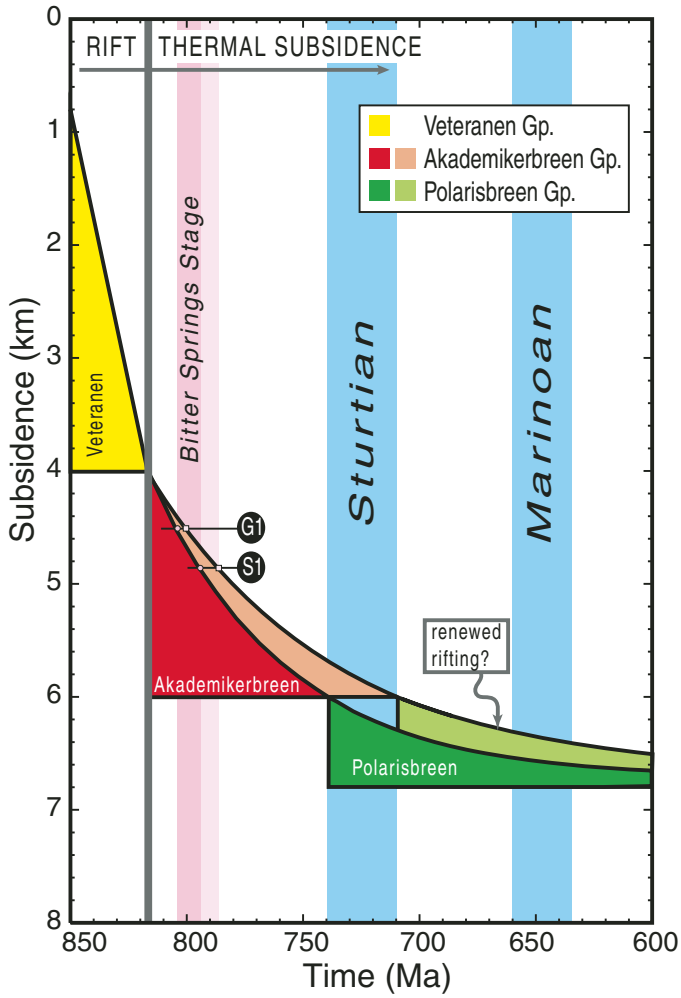

Figure 10. Age model for the Hecla Hoek strata of East Svalbard. The black curves show rifting (Veteranen Group) and thermal subsidence (Akademikerbreen Group) of an originally 35-km-thick continental crust and 100-km-thick lithosphere. The dark/light colored triangular areas beneath the solid curves depict the age distribution of the continuum of stratigraphic levels assuming onset of Sturtian glaciation at ca. 740 and ca. 710 Ma, respectively. The Akademikerbreen Group was deposited in ~90 m.y., and the entire Bitter Springs Stage lasted ~12 m.y. Discussion of the Polarisbreen Group is beyond the scope of this paper; however, it is worth noting that the post-Sturtian subsidence curve is more complicated than shown and should incorporate both (1) compaction of Polarisbreen shales, and (2) the possibility of renewed rifting (Herrington and Fairchild, 1989).

POSSIBLE EXPLANATIONS OF THE PALEOMAGNETIC DATA

Rapid Plate Tectonic Rotation during Depositional Hiatus

Our paleomagnetic record across the G1 sequence boundary is consistent across three continuous stratigraphic sections (i.e., correlations across covered stratigraphic intervals are not necessary; Fig. 7) and rules out the possibility that the ≥55° discrepancy between paleomagnetic directions from the lGfm and uGfm is due to local tectonic rotation. However, perhaps the most obvious explanation for the paleomagnetic data is that G1 consumes a lengthy depositional hiatus that accommodated at least 1900 km of latitudinal plate motion, and a minimum of 2670 km of total plate motion (assuming the minimum longitudinal motion associated with rotation). Given <20 m.y., and likely ~12 m.y., for deposition of the entire Bitter Springs Stage based on correlations with Australia and the position of G1 on the thermal subsidence trajectory for the East Svalbard platform (Fig. 10), it is likely that G1 accounts for less than a few million years of nondeposition. If the minimum 2670 km of plate motion across G1 is assumed to have spanned the entire 12–20 m.y. duration of the Bitter Springs Stage, we calculate lower limit plate velocities of 14–22 cm/yr. If, on the other hand, the G1 sequence boundary occupied a more reasonable time span of 1–5 m.y., plate velocities would have averaged 54–270 cm/yr.

For comparison, Conrad and Hager (2001) suggested that bending stresses associated with the subduction of oceanic lithosphere impose a speed limit on plate tectonic motions of ~20 cm/yr. This theoretical rate is similar to the maximum speed with which India covered >5000 km on its Eurasian approach, prior to Himalayan collision in the early Cenozoic (e.g., Van der Voo, 1993; McElhinny and McFadden, 2000). The fastest plate observed on Earth today is the Luzon plate, which has a velocity of 8–10 cm/yr

(e.g., Lallemand et al., 2005). The relatively short duration for G1 would require plate velocities 2–25 times the theoretical and observed speed limit for continents, arguing against a plate tectonic origin for the paleomagnetic discordance across G1.

Magnetic Excursions

A second explanation notes the similarity between the lGfm and S4mb paleomagnetic directions and postulates that the uGfm direction represents a magnetic excursion (Gubbins, 1999). However, the presence of as many as four symmetric polarity reversals in the uGfm (Fig. 7) and the short characteristic duration of 2–10 k.y. for magnetic excursions (Langereis et al., 1997) argues strongly against this hypothesis.

Nongeocentric Axial-Dipole Magnetic Fields

The paleomagnetic data could also be interpreted as a departure from a stable geocentric axial-dipole field, which would allow large paleomagnetic anomalies without rapid plate motions. The geometry of axial-centric quadrupolar and octupolar fields (Merrill et al., 1998; Kent and Smethurst, 1998; Bloxham, 2000) could not explain the large shift in paleomagnetic declination without larger changes in inclination across G1. A precessing equatorial dipole could explain the paleomagnetic data completely. So far, such a solution has only been found to be metastable in planetary bodies where the electrically conducting fluid core does not convect vigorously (Ishihara and Kida, 2000, 2002; Aubert and Wicht, 2004). Convection in the outer core is thought to be driven both by chemical and thermal buoyancy (Lister and Buffet, 1995; Kutzner and Christensen, 2000). Could the chemical composition of the outer core (controlled by growth of the inner core) or the thermal conditions at the core-mantle boundary (controlled by mantle circulation patterns influenced by a long-lived equatorial supercontinent) have retarded outer-core convection sufficiently to have stabilized a precessing equatorial dipole in the Neoproterozoic? This question is worth addressing in future magneto-hydrodynamic modeling experiments but is beyond the scope of this contribution.

True Polar Wander

We show here that, assuming an approximately stable geocentric axial-dipole field, a pair of rapid, oscillatory true polar wander events can explain the peculiar paleomagnetic record from lGfm to uGfm to S4mb. Furthermore, we show that, unlike the plate tectonic, magnetic excursion, or nongeocentric axial-dipole field hypotheses, the true polar wander hypothesis is consistent with plausible explanations for coincident excursions in $\delta^{13}C$ and relative sea level.

Paleogeography and the Location of I_{min}

Figure 11 details the paleogeographic evolution of Rodinia through the proposed true polar wander events across G1 and S1. The reconstruction at 1070 Ma is drawn to show the paleomagnetic constraints on the particular Rodinia configuration considered here (Appendix C). The exact geometry of Rodinia is a contentious issue (e.g., Hoffman, 1991; Dalziel, 1991; Weil et al., 1998; Karlstrom et al., 1999; Piper, 2000; Sears and Price, 2000; Buchan et al., 2001; Hartz and Torsvik, 2002; Wingate et al., 2002; Pisarevsky et al., 2003; Torsvik and Rehnström, 2003), but the first-order concept that Rodinia was centered around Laurentia and was in low latitudes is fairly well accepted and in many ways sufficient for this discussion.

At 805 Ma (with the lGfm pole aligned with the paleo–north pole) and for the preceding 50 m.y., ~80% of the continental area was located in the tropics. The G1 true polar wander event caused a 55° clockwise rotation of Rodinia, driving Siberia, Australia, India, South China, and part of Baltica out of the tropics and leaving <40% of the land area in the tropics by 800 Ma. A second true polar wander event, corresponding to S1, at ca. 790 Ma returned Rodinia to its "ringworld-like" position around the equator. By 750 Ma, the East Gondwanan cratons had begun spalling off the rift margin of western Laurentia. Much of the continental land area remained in the tropics and subtropics and left the world vulnerable to global glaciation (Donnadieu et al., 2004).

The I_{min} calculated by finding the pole to the great circle fit through the lGfm, uGfm, and S4mb poles is located in Ungava, Canada, statistically very close to the position of I_{min} found by Li et al. (2004) after fitting a great circle through the two South China poles (802 and 748 Ma). However, Li et al. (2004) inferred a single episode of counterclockwise true polar wander between 800 and 750 Ma, which drove a positive mass anomaly associated with the sub–East Gondwanan–West Laurentian superswell (expressed as 827–779 Ma mafic volcanism) from high latitudes to the equator.

The Li et al. (2004) paleomagnetic data are remarkably consistent with the Svalbard data presented here and the Rodinia paleogeography depicted in Figure 11. The 802 Ma pole for South China lies directly on the uGfm pole from Svalbard, further supporting the Bitter Springs Stage correlation between Svalbard and Australia and the argument that G1 occurred ca. 800 Ma. The position of the 748 Ma pole for South China (Fig. 11; 750 Ma) probably reflects a combination of the S1 true polar wander event and plate tectonic motion associated with the dispersal of East Gondwana and the breakup of western Rodinia. This scenario is consistent with the geometry of the 785–723 Ma apparent polar wander path for Laurentia (Fig. 11; 790 Ma) and predicts that the relative distances between the 748 Ma South China, 755 Ma Australia, 751 Ma India, and the interpolated 750 Ma Laurentian poles are due to relative plate motions (Fig. 11; 750 Ma). Well-documented rifting of the western Laurentian and East Gondwanan margins ca. 780 Ma and subsequent reamalgamation of the western Rodinian cratons into East Gondwana by 600–550 Ma are consistent with the hypothesis that paleomagnetic poles from these continents should begin to diverge by ca. 780–740 Ma. An alternative interpretation suggests that the great circle fit through the ca. 750 Ma

Figure 11. Paleogeographic reconstructions of the Rodinian supercontinent at 1070 Ma, 805–790 Ma, during the proposed true polar wander events, and 750 Ma during western Rodinia breakup (see Appendix C for details). Gray shading indicates the latitudinal extent of the tropics. The true polar wander spin axis (I_{min}) and its associated great circle are labeled in red, with the sense of motion marked with an arrow at the end of the I_{min} vector. Active/previous polar wander path segments are labeled with semitransparent pink-gray arrows. The schematic stratigraphic column (blue—carbonate deposition; black—karstic erosion; hachured—nondeposition) shows generalized relative sea level (green) and carbon-isotope (red) variability for East Svalbard, linked temporally to changing paleogeographies. Possible Rodinia geometries are varied and highly contentious, but the particular reconstructions depicted here are consistent with the generally accepted view that Rodinia was a long-lived supercontinent, which was centered around Laurentia and occupied low latitudes. It is important to note that precise paleogeographies for Rodinia are not generally agreed upon, nor are they critical to our general discussion of the interaction between true polar wander, eustasy, and $\delta^{13}C$.

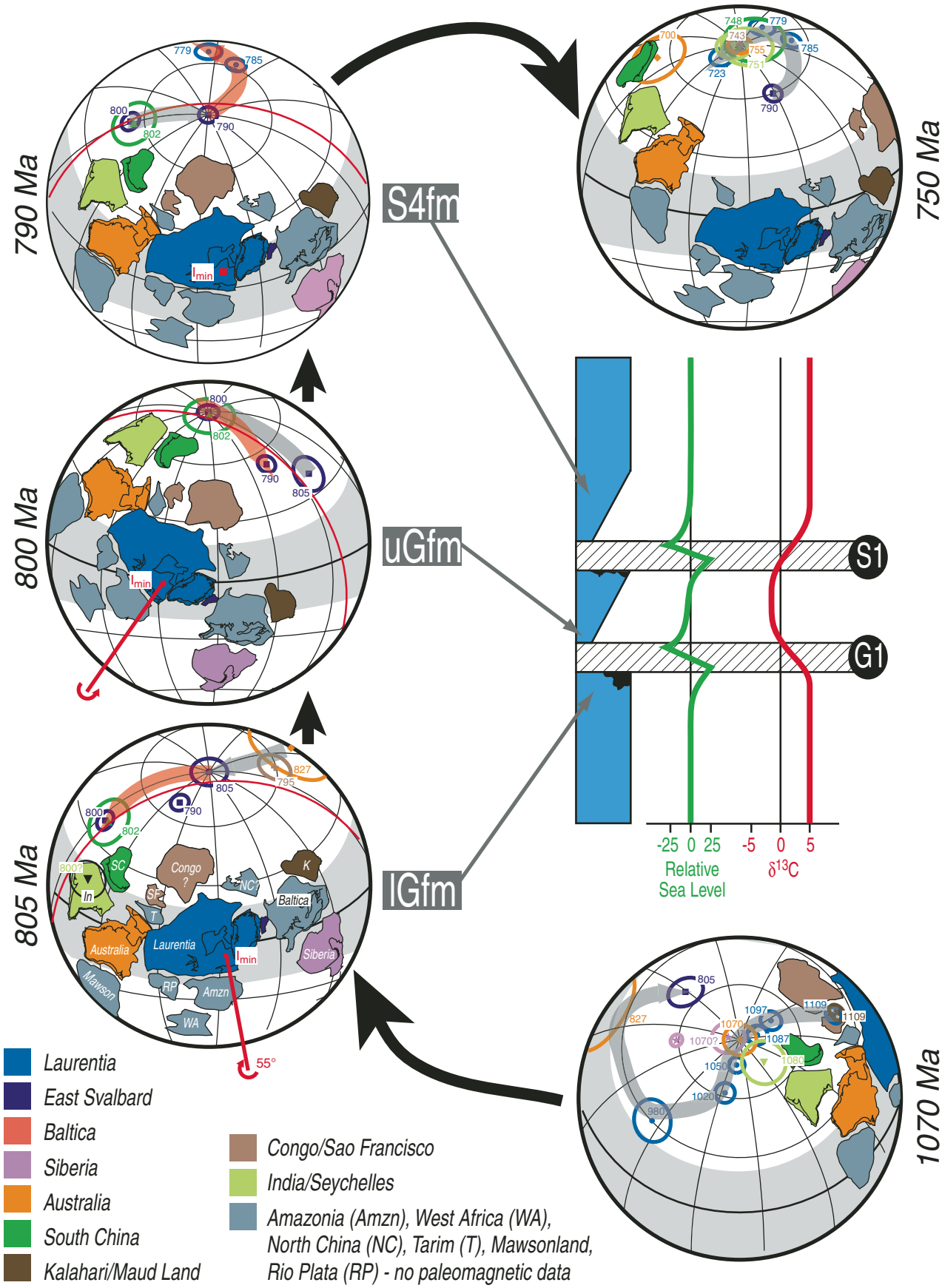

poles from Australia, India, and South China has caught a third inertial interchange true polar wander event (or a continuation of the S1 event) in action. We favor the first interpretation since it supports the idea of ca. 780 Ma rifting in western Rodinia, and it is potentially more consistent with the relative sea level and $\delta^{13}C$ records from East Svalbard.

Either hypothesis is consistent with the model of Evans (1998, 2003), where a long-lived supercontinent shields the underlying mantle from the cooling effects of subducted slabs, leading to an axis of mantle upwelling complementary to the girdle of downwellings associated with subduction zones encircling the supercontinent. In the Middle Neoproterozoic, this axis of mantle upwelling was located beneath eastern Rodinia, coaxial with I_{min}. Li et al.'s (2004) hypothesis would call for the rise of a subordinate mantle upwelling associated with the breakup of western Rodinia at 827–779 Ma, which may have caused the rotational instability at 800 Ma and the true polar wander events described here.

Relative Sea Level

As shown in the schematic East Svalbard stratigraphy (Fig. 11), the true polar wander hypothesis predicts that during each true polar wander event, East Svalbard first experiences a sea-level rise as the continent moves toward the equator, and then a sea-level fall as the platform crosses the equator and moves poleward. This general sea-level prediction is in direct agreement with stratigraphic observations made in the field where the G1 karstic unconformity suggests ~20 m of sea-level fall. Furthermore, the model of Mound et al. (1999) for a rapid true polar wander event (<10 m.y.) and average lithospheric thicknesses and mantle viscosities is consistent with the magnitude and timing of sea-level changes inferred from field observations. G1 and S1 are characterized by intervals of nondeposition and karstification of the underlying carbonate platform during sea-level fall. Any transgressive sediments deposited during the initial sea-level rise at the onset of true polar wander would be removed during the subsequent regression. The first sediments above G1 (uGfm) were deposited after the true polar wander event as the mantle and lithosphere relaxed and sea level rose again to equilibrium levels.

Because a true polar wander event will affect relative sea level on every continent differently, but predictably, depending on the continent's changing position relative to Earth's spin vector, the true polar wander hypothesis is testable using the stratigraphic record. For example, during G1, the thick carbonate platform of the Shaler Group on Victoria Island in the Canadian arctic (e.g., Rainbird et al., 1996; Asmerom et al., 1991) should have moved through only a few degrees of latitude toward the equator and thus experienced just a small sea-level rise. Therefore, the Shaler Group should record the full paleomagnetic declination and carbon-isotopic excursion without depositional hiatus. In contrast, the Bitter Springs Group of south-central Australia (e.g., Hill and Walter, 2000; Hill et al., 2000a; Southgate, 1989) should have traversed ~40° of latitude and experienced not only a large sea-level fall, but also a move from the tropics to the subtropics and a major increase in aridity.

The true polar wander events proposed here are rapid enough (<10 m.y.) that their influence on the relative sea-level signal should be visible in these and other stratigraphic records, despite the complicating effects of ambient tectonics and climate change. As will be demonstrated in the following section, the carbon isotope record should be globally uniform and could be used as a time marker to locate the G1 and S1 horizons in other basins that are not radiometrically dated.

Carbon Isotope Record

For intervals >1 m.y., a steady-state carbon-isotopic mass balance for bulk earth can be written as

$$\delta^{13}C_v = (1 - f_{org})\,\delta^{13}C_c + (f_{org})(\delta^{13}C_c - \varepsilon), \quad (1)$$

where $\delta^{13}C_v$ is the isotopic composition of the mantle, $\delta^{13}C_c$ is the isotopic composition of the inorganic carbon pool in the ocean derived from silicate weathering, ε is the fractionation between dissolved inorganic carbon (DIC) and dissolved organic carbon (DOC) (mostly due to the kinetic isotope effect associated with the uptake of carbon by photoautotrophs), and f_{org} ($= C_{org}/C_{total}$) is the fraction of carbon buried that is organic (Kump, 1991; Hayes et al., 2001). Carbonate burial due to carbonate weathering is ignored in this treatment because, over millions of years, carbonate weathering represents a simple transfer of carbonates from land to ocean, resulting in no net change of carbon in the ocean-atmosphere system. For the Middle Neoproterozoic, the carbonate being weathered from the continents will either have similar or lower $\delta^{13}C$ values compared to the new carbonate being deposited, and will, at most, lead to a small buffering effect against positive changes in carbon isotope mass balance.

Today, $\delta^{13}C_c \approx 0‰$, $\varepsilon \approx -25‰$, and $f_{org} \approx 0.2$. Assuming that ε remains approximately constant through time, an f_{org} of 0.4 would have been required to maintain Middle Neoproterozoic oceans with mean $\delta^{13}C_c$ of ~5‰ (Fig. 1D). Over the ≥200 k.y. time scale required to achieve carbon isotopic steady state, phosphate (PO_4^{2-}) is likely to be the limiting nutrient for primary productivity (Broecker and Peng, 1982; Smith, 1984; Lenton and Watson, 2000; Tyrrell, 1999; Schrag et al., 2002). It follows that the burial of organic carbon is controlled by the riverine flux of PO_4^{2-} to the ocean and the carbon to phosphorous (C:P) ratio of organic carbon that is buried (Kump, 1988; Schrag et al., 2002). As pointed out by Schrag et al. (2002) and Junge et al. (1975), an increase in silicate weathering would lead to an increase in the flux of both riverine PO_4^{2-} and alkalinity to the oceans, enhancing the burial of organic and carbonate carbon in approximately equal proportions and keeping f_{org} the same. Therefore, the steady-state $\delta^{13}C$ of carbonate rocks strongly reflects the globally averaged ratio of PO_4^{2-} to alkalinity released by the weathering of crustal rocks. Because the average composition of continental crust has not changed by large amounts since 3 Ga, mean $\delta^{13}C$ of carbonates has been relatively constant through time (with a few exceptions in the Paleoproterozoic, Neoproterozoic, Cambrian, Permian-Carboniferous, and Early Triassic). If the composition of the crust has not changed much through time, then sustained, anomalously positive $\delta^{13}C$ values in the Middle Neoproterozoic ocean must have been maintained by other processes, such as increases in the C:P ratio in buried organic matter. Barring large fluctuations in the Redfield ratio of primary organic matter through time, the C:P ratio of buried C_{org} depends on the state of oxygenation at the burial site, with local anoxia favoring remobilization of PO_4^{2-} and efficient burial of low C:P organic carbon (Ingall and Van Cappellen, 1990; Ingall et al., 1993; Van Cappellen and Ingall, 1996; Ingall and Jahnke, 1997). Global bottom water anoxia is a possibility, although the ocean mixing required to return liberated PO_4^{2-} from bottom waters to the photic zone results in a return flow that that may keep the ocean variably oxidized, depending on the magnitude of the oxygen source in the atmosphere and the oxygen sinks in the ocean. However, even in a partly oxidized world, coupled sites of rapid organic carbon burial and local anoxia could be maintained to substantially lower C:P in globally averaged sedimentary organic carbon.

Today, some 70% of the total organic carbon removed from the global ocean-atmosphere-terrestrial biosphere system is buried in the sediments of large tropical river deltas such as the Amazon and those in southeast Asia (Hedges and Keil, 1995; Berner, 1982). Although some of the organic carbon that is buried was derived as particulate terrestrial organic matter carried as suspended load to the ocean, much of the organic carbon that is buried is marine in origin (Aller et al., 1996). Tropical river systems drain

catchments undergoing rapid silicate weathering due to the positive temperature and moisture dependence of chemical weathering rates (Berner et al., 1983). These rivers deliver abundant nutrients to the ocean, assuring high productivity. The same rivers also provide huge volumes of physically weathered sediment, some of which adsorbs to particulate organic matter in the water column (Keil et al., 1994; Mayer, 1999) and buries it before it can be oxidized. Even in the absence of a substantial terrestrial biosphere during the Neoproterozoic, tropical river deltas would still have been a dominant site for organic carbon burial. Schrag et al. (2002) postulated that the abundance of equatorial land area during the Middle Neoproterozoic (Fig. 11; 805, 790, and 750 Ma) would have led to a greater number of tropical river systems, more restricted equatorial ocean basins experiencing at least local bottom water anoxia, and a corresponding increase in f_{org}, which would have led to the steady state characterized by strongly positive surface ocean $\delta^{13}C$.

The shift in $\delta^{13}C$ from an average of +6‰ to –1.5‰ across G1 can be understood as the steady-state response to a drastic reduction in f_{org} (from 0.4 to 0.14) caused by true polar wander–induced motion of vast tropical land areas toward the poles. Figure 11 (800 Ma) shows how the 55° clockwise rotation of Rodinia across G1 would have stranded large tropical river systems draining Grenville-age (1.3–0.95 Ga) orogenic systems, such as the Albany-Fraser belt of southwestern Australia, the Jiangnan belt of South China, the Eastern Ghats of eastern India, the Sveconorwegian belt of southwest Baltica, and the Namaqua-Natal belt of southern Kalahari in the drier subtropics or colder temperate regions. These once-tropical river deltas, which were sites of high productivity, bottom-water anoxia, and rapid C_{org} burial, would have become lower-productivity, more oxic subtropical or temperate depocenters with lower sedimentation rates and less effective organic carbon burial. The abrupt switch back to enriched $\delta^{13}C$ across S1 and the similarity in paleomagnetic poles from lGfm and S4mb together support the idea that a second true polar wander event of equal magnitude may have reestablished the Middle Neoproterozoic preponderance of low-latitude continents (Fig. 11; 790 Ma).

Rothman et al. (2003) proposed that large fluctuations in Neoproterozoic $\delta^{13}C$ were due to non-steady-state interactions between the marine inorganic carbon pool and an unusually large, isolated C_{org} reservoir that was mixed periodically with the surface ocean (see also, Grotzinger and Knoll, 1995). The C_{org} pool required to cause the Bitter Springs Stage is more than three orders of magnitude greater than the modern oceanic dissolved and particulate C_{org} reservoir and more than 20 times larger than the modern oceanic reservoir of total carbon. Although it is not clear how or why such a large isolated, but accessible, reservoir of organic carbon could have been maintained for hundreds of millions of years, a true polar wander event may have been an effective means of mixing the carbon reservoirs and causing $\delta^{13}C_c$ excursions. The Rothman et al. (2003) mechanism for negative $\delta^{13}C$ excursions may or may not have been important during the Middle Neoproterozoic, but could be tested if reliable $\delta^{13}C_{org}$ records are retrieved from planktonic and benthic organic matter spanning the Bitter Springs Stage.

Kirschvink and Raub (2003) suggested that the release of isotopically light methane through the destabilization of frozen clathrates on continental slopes during true polar wander–induced sea-level and ocean circulation changes could be responsible for large $\delta^{13}C$ excursions. However, methane release could not have caused the ~7‰ shift in $\delta^{13}C$ during the Bitter Springs Stage because the volume of methane required to maintain the 12 m.y. excursion is more than an order of magnitude greater than the potential global reservoir of methane clathrate (Kvenvolden, 1999; Buffett, 2000; Dickens, 2001; Buffett and Archer, 2004). It is possible that methane releases during inertial interchange true polar wander events led to $\delta^{13}C$ variability over much shorter time scales, but such behavior is not observed in East Svalbard.

CONCLUSIONS

New paleomagnetic data from Middle Neoproterozoic strata of East Svalbard fill an important gap in the Laurentian apparent polar wander path from ca. 810 to 790 Ma. Two 55° shifts in paleomagnetic orientation coincide with the only two large transient sea-level fluctuations (G1 and S1) observed in the 2-km-thick sedimentary record of East Svalbard. The paleomagnetic and sea-level shifts bracket a prolonged ~7‰ negative carbon isotope excursion, called the Bitter Springs Stage, that is preserved in at least two cratons.

Our most parsimonious interpretation is that the inferred 4 cm/yr of polar motion between sedimentary units below (lGfm) and above (S4mb) the Bitter Springs Stage is due to plate tectonics, while the abrupt 54–270 cm/yr paleomagnetic reorientations into (G1) and out of (S1) the Bitter Springs Stage are a pair of true polar wander events. The true polar wander events were centered around a minimum inertial axis beneath eastern Rodinia, and may have been excited by the growth of a subordinate mantle upwelling beneath western Rodinia related to the rifting of the East Gondwanan continents from the western margin of Laurentia.

Transient relative sea-level drops of >10 m on thermally subsiding platforms can be caused either by the growth or decay of ice sheets or changes in the magnitude or orientation of Earth's spin vector. If sea-level drops are due to changes in ice volume, boundaries like G1 and S1 should be abundant, they would be likely to recur at Milankovitch frequencies, and they should be associated with glacial deposits somewhere on the globe. The sea-level fluctuations observed in East Svalbard are more consistent with the magnitude and time scale of true polar wander–induced sea-level changes.

The ~7‰ negative carbon isotope excursion was caused by a large change in carbon fluxes and likely represents a shift in the ratio of organic carbon to total carbon burial (f_{org} changes from 0.4 to 0.14). The preponderance of equatorial land area in the Middle Neoproterozoic gave rise to a unique situation where effective sites of organic carbon burial, such as tropical river deltas, were abundant and f_{org} was quite high. This interval from ca. 900 to 740 Ma is the longest period in Earth history with average $\delta^{13}C_c \geq 5‰$. The true polar wander across G1 drove about half of the equatorial land area out of the tropics, reducing the number of sites for efficient organic carbon burial, and driving f_{org} and $\delta^{13}C_c$ down. The second true polar wander event across S1 reestablished the tropical Rodinia configuration and returned $\delta^{13}C_c$ to the strongly positive values typical of the Middle Neoproterozoic.

If the true polar wander hypothesis for the Bitter Springs Stage is correct, then all continents that preserve ca. 800 Ma strata may preserve predictable records of sea-level fluctuation and carbon isotopic and paleomagnetic excursions correlative to G1 and S1. In fact, independent determination of the relative position of I_{min} to individual cratons could place new geographic constraints on reconstructions of Rodinia.

APPENDIX

A. Paleomagnetic and Rock Magnetic Methods

Paleomagnetics

Block samples were oriented in the field using a Brunton compass, and were later cored in the laboratory. Sun compass observations were made whenever possible to ensure an accurate measure of the local magnetic declination. Remnant magnetization measurements were made with a 2G Enterprises™ DC SQuID magnetometer with background noise sensitivity of 5×10^{-12} A m^2 per axis. The magnetometer was equipped with computer-controlled, online altering field (AF) demagnetization coils and an automated vacuum pick-and-put sample changing array (Kirschvink, 2002). Samples and instruments were housed in a magnetically shielded room with residual fields

<100 nT throughout the demagnetization procedures. After measuring the natural remanent magnetization (NRM) of all samples, a subset of samples was demagnetized cryogenically in a low-magnetic field bath of liquid nitrogen in order to remove any fields that may have been acquired during the passage of hematite through the Morin transition, and to help unblock larger multidomain magnetite grains by cycling through the Verwey transition. Next, random magnetic field components were removed from all samples via stepwise AF demagnetization at 2.5, 5.0, 7.5, and 10.0 mT. Finally, all samples were thermally demagnetized in steps of 5–50 °C up to 670 °C (or until thoroughly demagnetized, for an average of 20–25 thermal steps per specimen) in a magnetically shielded ASC™ oven (±2 °C error) in a nitrogen atmosphere. After each demagnetization step, three-axis measurements were made in both sample-up and sample-down orientations, and samples with circular standard deviation >10° were rerun manually. Magnetic components were computed for each sample using principal component analysis (Kirschvink, 1980) as implemented in PaleoMag OS X (Jones and Tetreault, 2004).

Low-Temperature Cycling

A Quantum Designs Magnetic Property Measurement System (MPMS) superconducting quantum interference device (SQUID) magnetometer was used to measure low-temperature magnetism in Svalbard rocks at the Center for Material Sciences and Engineering (CMSE) at Massachusetts Institute of Technology (MIT). The low-temperature cycling experiments on 0.2–4.0 g samples proceeded as follows: (1) a saturating 1 T field at 300 K was applied; (2) the field was quenched to ≤0.2 mT; (3) magnetic moment in the sample was measured as it cooled to 10 K in 3–10 K increments; and (4) magnetic moment in the sample was measured as it warmed back to 300 K in 3–10 K increments.

At ~120 K, magnetite undergoes a phase transition from a high-temperature cubic phase to a low-temperature monoclinic phase. This phase change, called the Verwey transition, will occur at lower temperatures for impure or partially oxidized magnetite. When magnetite is cooled through the Verwey transition, it demagnetizes, but recovers some fraction of its original remanence when warmed back to room temperature. The ratio of the remanence before and after low-temperature cycling through the Verwey transition depends on the crystal size and domain state of the magnetite grains. Reversible increases in remanence upon cooling from 30 K to 10 K in a nonzero field are commonly attributed to the presence of very small magnetite grains (30 nm) that are superparamagnetic (SP) at 300 K.

Hysteresis

Both a Quantum Designs MPMS at the MIT Center for Materials Science and Engineering and an ADE vibrating sample magnetometer (VSM) in the Ross Laboratory in the MIT Department of Materials Science and Engineering were used to generate hysteresis loops for Svalbard rocks. The samples were placed in a saturating field of 1 T, and magnetic moments were measured as the applied field cycled between 1 T and –1 T in 5–50 mT steps.

Although multidomain (MD) grains (and 300 nm) may respond to applied magnetic fields by domain wall displacement, nucleation, and/or rotation, SD grains (≤30–80 nm) can only rotate. Domain rotation is resisted by both magnetic and crystalline anisotropy and is therefore a higher-energy process than displacement or nucleation (Dunlop and Özdemir, 1997). For these reasons, a much larger applied field is required to change the magnetization in an SD grain than in an MD grain. Hysteresis loops are constructed by cycling samples through increasing and decreasing applied fields. The resulting plot of acquired magnetic moment versus applied field can be used to measure the coercive force required to reduce the sample's magnetic moment to zero (B_c), as well as the ratio of saturation remanence (M_{rs}) to saturation magnetization (M_s). MD magnetite grains should have lower coercivities and lower M_{rs}/M_s than SD magnetite. Hematite grains will have much higher coercivities than magnetite grains.

Electron Microprobe

Two representative samples from lGfm, uGfm, and S4mb were also examined using the MIT Center for Geochemical Analysis Electron Probe X-ray Microanalyzer (EMPA) with 1 μm resolution. The EMPA can quantify the shape and composition of MD magnetic grains if they exist.

B. Subsidence Model

The model accepts as inputs y_{sr}, the average thickness of rift sediments, y_c, the average thickness of the continental crust, and y_l, the average thickness of the continental lithosphere. The term ρ_{sr} is the density of the synrift sediments. Densities of the crust and mantle are temperature dependent. T_c, T_{sc}, and T_m are the average temperatures of the crust, the subcrustal lithosphere, and the asthenospheric mantle, respectively, and define a simplified lithospheric geotherm. Then

$$\rho_c(T) = \rho_c(1 - \alpha T_c) \quad (2)$$

is the average density of the continental crust,

$$\rho_{sc}(T) = \rho_m(1 - \alpha T_{sc}) \quad (3)$$

is the average density of the subcrustal lithosphere, and

$$\rho_m(T) = \rho_m(1 - \alpha T_m) \quad (4)$$

is the average density of the asthenospheric mantle, where α is the coefficient of thermal expansion. Using this information, an equation for isostatic equilibrium before stretching and after instantaneous rifting/filling can be derived in order to calculate the stretching factor, $\beta = y_l'/y_l$, where y_l' is the thickness of the lithosphere after uniform crustal stretching:

$$\beta = \frac{\rho_c(T)y_c + \rho_{sc}(T)(y_l - y_c) - \rho_m(T)y_l}{\rho_c(T)y_c + \rho_{sc}(T)(y_l - y_c) - \rho_{sr}y_{sr} + \rho_m(T)(y_{sr} - y_l)}. \quad (5)$$

Once β is determined, the model generates a function, $S(t)$, which calculates the accumulation of sediments, y_{st}, of density ρ_{st}, in the accommodation space created by thermal subsidence of the continental lithosphere with time:

$$S(t) = E_0 \frac{\beta}{\pi} \sin\left(\frac{\pi}{\beta}\right)\left(1 - e^{\frac{-t}{\tau}}\right) \cdot 10^{-3}, \quad (6)$$

where

$$E_0 = \frac{4y_l\rho_m\alpha T_m}{\pi^2(\rho_m - \rho_{st})}, \quad (7)$$

$$\tau = \frac{y_l^2}{\pi^2\kappa}, \quad (8)$$

and κ is the coefficient of thermal diffusivity (Allen and Allen, 1990). Because the thermal subsidence sediments are composed entirely of early-cemented carbonates, we assumed that compaction during burial was negligible. Our first-order model used y_{sr} = 4 km, y_{st} = 2 km, y_c = 35 km, y_l = 100 km, ρ_{sr} = 2060 kg m^{-3} (sandstone), ρ_{st} = 2500 kg m^{-3} (mixed limestone and dolomite), ρ_c = 2700 kg m^{-3}, ρ_m = 3300 kg m^{-3}, T_0 = 0 °C, T_m = 1333 °C, α = 3.28 10^{-5} °C^{-1}, and κ = 10^{-6} m^2 s^{-1}.

C. Paleomagnetic Constraints on Rodinia

Paleogeographic reconstructions of the Rodinian supercontinent at 1070 Ma, 805–790 Ma during the inferred true polar wander events, and 750 Ma during breakup are shown in Figure 11. In each equal-area plot (generated using Cogné, 2003), a light-gray band shows the location of the tropics. Paleopoles are color-coded to their host cratons, where numbers show their ages in Ma, and they are listed in Table 2. Cratons with no reliable paleomagnetic data are colored gray.

In Figure 11, the 1070 Ma Rodinia reconstruction shows the available paleomagnetic constraints from ca. 1110 to 800 Ma (Table 2). Euler poles for rotating each craton into present-day Laurentian coordinates are collected in Table 3.

Pre–1000 Ma poles from India, Australia, Kalahari, and to some extent, Siberia, are rotated until they fall on the Logan Loop (Laurentia 1109–1020 [Halls and Pesonen, 1982]). Kalahari is positioned so that the Namaqua-Natal belt is a continuation of the Sveconorwegian belt of Baltica, and the Umkondo dikes are included in the vast area of 1110–1070 Ma mafic volcanism behind the Grenville front. Siberia is rotated until its northern margin is separated from northwestern Baltica by a narrow Ægir Sea (Hartz and Torsvik, 2002). South China and East Svalbard share a paleomagnetic pole at ca. 800 Ma (see 805 Ma reconstruction), and the present-day southeast margin of South China faces the Lesser Himalaya of India (Jiang et al., 2003). The Neoproterozoic rift margin of southwestern Congo–Sao Francisco is positioned off northwestern Laurentian, putting the ca. 795 Ma pole from Congo somewhat close to and between the 805 Ma East Svalbard and 827 Ma Australian poles (see 805 Ma reconstruction). Tarim is located off western Laurentia so that the rift succession of the Quruqtagh in Xinjiang province (Norin, 1937; Xiao et al., 2004) faces the rifted margin of the North American Cordillera. Tarim might represent the fragment that stayed near western Laurentia (750 Ma reconstruction) until final separation in the latest Neoproterozoic–Early Cambrian (Bond and Kominz, 1984; Bond et al., 1984). The northern margin of the North China block is located off north Laurentia as the missing craton that rifted away from the Inuitian margin of Laurentia in the Early Cambrian. The inverted Baltica fit of Hartz and Torsvik (2002) helps explain the tectonic origin of the Southern peri Urals and East Greenland East Svalbard (SPUEGES) platform and removes the necessity of some Paleozoic gymnastics during the opening of the Iapetus ocean (Torsvik et al., 1996; Torsvik and Rehnström, 2001). However, this inverted fit places the ca. 1050 ± 30 Ma pole far from the Logan Loop and locates the nearly stationary group of 980–850 Ma poles southeast of the 980 Ma Laurentian pole (not shown in Figure 11; 1070 Ma). The Baltica right-way-up fit of Pisarevsky et al. (2003) is more consistent with the existing paleomagnetic data, although none of the Baltica poles have positive paleomagnetic field tests. Juxtaposing the Andean margin of Amazonia with the Grenville margin of eastern

TABLE 2. PALEOMAGNETIC POLES USED TO RECONSTRUCT RODINIA

Pole ID	Latitude (°N)	Longitude (°E)	*dp*	*dm*	Age (Ma)	Reference
Laurentia						
Logan sills	49.0	220.0	4.0	4.0	1109 ± 2	Halls and Pesonen (1982); Davis and Sutcliffe (1985)
Upper North Shore volcanics	32.0	184.0	5.0	5.0	1097 ± 2	Halls and Pesonen (1982); Davis and Green (1997)
Lake Shore traps	22.0	181.0	5.0	5.0	1087 ± 2	Diehl and Haig (1994); Davis and Paces (1990)
Nonesuch Shale	8.0	178.0	4.0	4.0	1050 ± 30	Henry et al. (1977); Wingate et al. (2002)
Freda sandstone	2.0	179.0	4.0	4.0	1050 ± 30	Henry et al. (1977); Wingate et al. (2002)
Jacobsville sandstone	–9.0	183.0	4.0	4.0	1020 ± 30	Roy and Robertson (1978)
Chequamegon sandstone	–12.0	178.0	5.0	5.0	1020 ± 30	McCabe and Van der Voo (1983)
Haliburton intrusion	–36.0	143.0	10.0	10.0	980 ± 10	Buchan and Dunlop (1976)
Wyoming dikes	13.0	131.0	4.0	4.0	785 ± 8	Harlan et al. (1997)
Tsezotene sills	2.0	138.0	5.0	5.0	779 ± 2	Park et al. (1989); LeCheminant and Heaman (1994)
Franklin dikes	5.0	163.0	5.0	5.0	723^{+4}_{-2}	Heaman et al. (1992); Park (1994)
East Svalbard						
IGfm	19.6	211.3	2.2	4.2	ca. 810	Table 1
uGfm	2.6	71.9	1.4	2.8	ca. 800	Table 1
S4mb	25.9	226.8	4.3	7.7	ca. 790	Table 1
Baltica						
Laanila dolerite	–2.0	212.0	15	15	1045 ± 50	Mertanen et al. (1996)
Gallared granite	–44.0	224.0	6	6	985 ± 5	Pisarevsky and Bylund (1998); Möller and Söderlund (1997)
Gallared amphibolite	–46.0	214.0	19	19	ca. 956	Pisarevsky and Bylund (1998); Möller and Söderlund (1997)
Egursund anorthosite	–44.0	214	4	4	930 ± 2	Stearn and Piper (1984); Torsvik and Eide (1997)
Hunnedalen dikes	–41.0	222.0	10	10	ca. 848 ± 27	Walderhaug et al. (1999)
Siberia						
Turukhansk red beds	–15.0	256.0	8	8	975–1100	Gallet et al. (2000)
Uchur-Maya red beds	–25.0	231	3	3	990–1150	Gallet et al. (2000)
Australia						
Bangemall sills	34.0	95.0	8	8	1070 ± 6	Wingate et al. (2002)
Mundine Well dikes	45.0	135.0	4	4	755 ± 3	Wingate and Giddings (2000)
Wooltana volcanics	–62.0	142.0	16.0	16.0	827 ± 6?	McWilliams and McElhinny (1980); Preiss (2000)
Walsh cap dolomite	–21.5	282.4	12.2	12.2	ca. 720	Li (2000)
South China						
Xiaofeng dikes	13.5	91.0	10.5	10.5	802 ± 10	Li et al. (2004)
Liantuo sediments	4.0	161.0	13	13	748 ± 12	Evans et al. (2000)
Kalahari						
Umkondo and Dronning Maud	37.4	63.2	3.8	3.8	1109 ± 1	Hanson et al. (2004); Powell et al. (2001); Wingate (2001); Jones et al. (2003)
Congo–São Francisco						
Gagwe lavas	25.0	93.0	10	10	795 ± 7	Meert et al. (1995); Deblond et al. (2001)
Mbozi gabbro	46.0	325.0	9	9	755 ± 25	Meert et al. (1995)
India–Seychelles						
Wajrakarur kimberlites	45.0	59.0	11	11	ca. 1079	Miller and Hargraves (1994)
Harohalli dikes	27.0	79.0	18	18	ca. 814 ± 34	Radhakrishna and Mathew (1996)
Malani igneous suite	68.0	88.0	8	8	761 ± 10	Torsvik et al. (2001b)
Mahe dikes	80.0	79.0	11	11	751 ± 3	Torsvik et al. (2001a)

TABLE 3. EULER POLE ROTATIONS INTO A RODINIA CONFIGURATION IN LAURENTIAN COORDINATES

Pole ID	Latitude (°N)	Longitude (°E)	Rotation (°)
Greenland	68	–119	–14
East Svalbard	–81	125	68
Baltica	–58	205	–112
Siberia	69	294	–92
Australia	55	150	120
South China	–88	45	–94
Kalahari	20	327	91
Congo-Sao Francisco	–6	278	128
India-Seychelles	–65	346	–154
Amazonia	17	318	–95
West Africa	15	325	172
Tarim	–10	158	–94
North China	–12	20	50

Laurentia is consistent with 1–5 cm yr^{-1} of northward drift of Amazonia between the ca. 1200 Ma emplacement of the Nova Floresta Gabbro (Tohver et al., 2002) and the 1.1–1.0 collision with Laurentia (Rivers, 1997). In the absence of new paleomagnetic or geologic constraints, West Africa, Rio de la Plata, and Mawsonland are positioned as in previous Rodinia reconstructions (e.g., Hoffman, 1991; Dalziel, 1991; Weil et al., 1998; Pisarevsky et al., 2003).

At 805 Ma, all cratons with the exception of Congo and West Africa, are within or straddling the tropics. The first inferred true polar wander event leads to the 800 Ma configuration, with Australia, Siberia, India, and South China moving out of the tropics. The second inferred true polar wander event returns most of Rodinia to the tropics ca. 790 Ma. By ca. 750 Ma, disparate poles from Australia, India, and South China suggest that East Gondwanan cratons had rifted away from the western margin of Laurentia.

ACKNOWLEDGMENTS

This work was supported by the National Science Foundation (Arctic Natural Sciences Research Program grant OPP-9817244), the National Aeronautics and Space Administration (NASA) Astrobiology Institute, the Canadian Institute for Advanced Research (Earth System Evolution Project), the Tectonics Special Research Centre (Perth, Australia), and the Agouron Institute. Critical reviews from John Geissman, Arlo Weil, Joseph Meert, David Bice, and Rob Van der Voo improved the manuscript. Additionally, the paper benefited from useful discussions with David Barbeau, Thorsten Becker, Michael Bender, Jeremy Blox-

ham, Sam Bowring, Bruce Buffett, Mathieu Dumberry, David Evans, David Fike, John Grotzinger, Ebbe Hartz, John Hayes, Matthew Hurtgen, David Jones, Jamie Kellogg, Andy Knoll, Francis Macdonald, Jerry Mitrovica, Jon Mound, Richard O'Connell, Ryan Petterson, Susannah Porter, Pascale Poussart, Timothy Raub, David Rowley, Jorge Sarmiento, John Suppe, Ben Sheets, Sabine Stanley, Nick Swanson-Hysell, Carl Tape, and Trond Torsvik. Jean-Pascal Cogné provided tireless support with his excellent paleomagnetics software. Norsk Polarinstitutt, Airlift, and the crew of the vessel *Farm* made Svalbard logistics more manageable. Cris Carman, Anne Estoppey, John Higgins, Matt Hurtgen, Leslie Hsu, Brice Jones, Peter Moore, and Meg Smith provided assistance in the field. Ethan Goddard and Greg Eischeid supervised the isotope laboratory work at Harvard University. Bob Kopp helped keep the paleomagnetics laboratory at Caltech running smoothly, while Roberta Bennett-Calorio made working at MIT a pleasure. Caroline Ross, Fernando Castaño, Debbie Morecroft, and Vikram Sivakumar facilitated vibrating sample magnetometer experiments and Fang Cheng Chou trained us on the Magnetic Property Measurement System (MPMS). Nilanjan Chatterjee and Tim Grove helped us with electron microprobe measurements.

REFERENCES CITED

Allen, P., and Allen, J., 1990, Basin analysis: Principles and applications: Oxford, UK, Blackwell Science, 451 p.

Aller, R., Blair, N., Xia, Q., and Rude, P., 1996, Remineralization rates, recycling, and storage of carbon in Amazon shelf sediments: Continental Shelf Research, v. 16, p. 753–786, doi: 10.1016/0278-4343(95)00046-1.

Alvarez, W., and Lowrie, W., 1978, Upper Cretaceous palaeomagnetic stratigraphy at Moria (Umbrian Apennines, Italy): Verification of the Gubbio section: Geophysical Journal of the Royal Astronomical Society, v. 55, p. 1–17.

Andrews, J., 1985, True polar wander: An analysis of Cenozoic and Mesozoic paleomagnetic poles: Journal of Geophysical Research, v. 90, p. 7737–7750.

Anson, G., and Kodama, K., 1987, Compaction-induced inclination shallowing of the postdepositional remanent magnetization in a synthetic sediment: Geophysical Journal of the Royal Astronomical Society, v. 88, p. 673–692.

Asmerom, Y., Jacobsen, S., Knoll, A., Butterfield, N., and Swett, K., 1991, Strontium isotopic variations of Neoproterozoic seawater: Implications for crustal evolution: Geochimica et Cosmochimica Acta, v. 55, p. 2883–2894, doi: 10.1016/0016-7037(91)90453-C.

Aubert, J., and Wicht, J., 2004, Axial vs. equatorial dipolar dynamo models with implications for planetary magnetic fields: Earth and Planetary Science Letters, v. 221, p. 409–419, doi: 10.1016/S0012-821X(04)00102-5.

Berner, R., 1982, Burial of organic carbon and pyrite sulfur in the modern ocean: Its geochemical and environmental significance: American Journal of Science, v. 282, p. 451–473.

Berner, R., Lasaga, A., and Garrels, R., 1983, The carbonate-silicate geochemical cycle and its effects on atmospheric carbon dioxide over the past 100 million years: American Journal of Science, v. 283, p. 641–683.

Besse, J., and Courtillot, V., 1991, Revised and synthetic polar wander paths of the African, Eurasian, North American, and Indian plates and true polar wander since 200 Ma: Journal of Geophysical Research, v. 96, p. 4029–4050.

Besse, J., and Courtillot, V., 2002, Apparent and true polar wander and the geometry of the geomagnetic field over the last 200 Myr: Journal of Geophysical Research, v. 107, p. 2300, doi: 10.1029/2000JB000050.

Bickle, M., Martin, A., and Nisbet, E., 1975, Basaltic and peridotitic komatiites, stromatolites and a basal unconformity in the Belingwe greenstone belt, Rhodesia: Earth and Planetary Science Letters, v. 27, p. 155–162, doi: 10.1016/0012-821X(75)90024-2.

Bills, B., and James, T., 1996, Late Quaternary variations in relative sea level due to glacial cycle polar wander: Geophysical Research Letters, v. 23, p. 3023–3026, doi: 10.1029/96GL02886.

Bingen, B., Demaiffe, D., and van Breemen, O., 1998, The 616 Ma old Egersund basaltic dike swarm, SW Norway, and Late Neoproterozoic opening of the Iapetus Ocean: The Journal of Geology, v. 106, p. 565–574.

Blake, T., Buick, R., Brown, S., and Barley, M., 2004, Geochronology of a Late Archean flood basalt province in the Pilbara Craton, Australia: Constraints on basin evolution, volcanic and sedimentary accumulation, and continental drift rates: Precambrian Research, v. 133, p. 143–173, doi: 10.1016/j.precamres.2004.03.012.

Bloxham, J., 2000, Sensitivity of the geomagnetic axial dipole to thermal core-mantle interactions: Nature, v. 405, p. 63–65, doi: 10.1038/35011045.

Bond, G., and Kominz, M., 1984, Construction of tectonic subsidence curves for the early Paleozoic miogeocline, southern Canadian Rocky Mountains: Implications for subsidence mechanisms, age of break-up, and crustal thinning: Geological Society of America Bulletin, v. 95, p. 155–173, doi: 10.1130/0016-7606(1984)95<155:COTSCF>2.0.CO;2.

Bond, G., Nickleson, P., and Kominz, M., 1984, Breakup of a supercontinent between 625 and 555 Ma: New evidence and implications for continental histories: Earth and Planetary Science Letters, v. 70, p. 325–345, doi: 10.1016/0012-821X(84)90017-7.

Bowring, S., Myrow, P., Landing, E., Ramezani, J., Condon, D., and Hoffmann, K., 2003, Geochronological constraints on Neoproterozoic glaciations and the rise of Metazoans: Geological Society of America Abstracts with Programs, v. 35, no. 6, p. 516.

Brasier, M., McCarron, G., Tucker, R., Leather, J., Allen, P., and Shields, G., 2000, New U-Pb zircon dates for the Neoproterozoic Ghubrah glaciation and for the top of the Huqf Supergroup, Oman: Geology, v. 28, p. 175–178, doi: 10.1130/0091-7613(2000)028<0175:NUPZDF>2.3.CO;2.

Breivik, A., Mjelde, R., Grogan, P., Shimamura, H., Murai, Y., Nishimura, Y., and Kuwano, A., 2002, A possible Caledonide arm through the Barents Sea imaged by OBS data: Tectonophysics, v. 355, p. 67–97, doi: 10.1016/S0040-1951(02)00135-X.

Broecker, W., and Peng, T.-H., 1982, Tracers in the sea: Eldigio Press, 681 p.

Buchan, K., and Dunlop, D., 1976, Paleomagnetism of the Haliburton intrusions: Superimposed magnetizations, metamorphism, and tectonics in the late Precambrian: Journal of Geophysical Research, v. 81, p. 2951–2966.

Buchan, K., Ernst, R., Hamilton, M., Mertanen, S., Pesonen, L., and Elming, S., 2001, Rodinia: The evidence from integrated palaeomagnetism and U-Pb geochronology: Precambrian Research, v. 110, p. 9–32, doi: 10.1016/S0301-9268(01)00178-4.

Buffett, B., 2000, Clathrate hydrates: Annual Review of Earth and Planetary Sciences, v. 28, p. 477–507, doi: 10.1146/annurev.earth.28.1.477.

Buffett, B., and Archer, D., 2004, Global inventory of methane clathrate: Sensitivity to changes in the deep ocean: Earth and Planetary Science Letters, v. 227, p. 185–199, doi: 10.1016/j.epsl.2004.09.005.

Cande, S., Raymond, C., Stock, J., and Haxby, W., 1995, Geophysics of the Pitman fracture zone and Pacific-Antarctic plate motions during the Cenozoic: Science, v. 270, p. 947–953.

Cawood, P., McCausland, P., and Dunning, G., 2001, Opening Iapetus: Constraints from the Laurentian margin in Newfoundland: Geological Society of America Bulletin, v. 113, p. 443–453, doi: 10.1130/0016-7606(2001)113<0443:OICFTL>2.0.CO;2.

Cogné, J., 2003, PaleoMac; a Macintosh™ application for treating paleomagnetic data and making plate reconstructions: Geochemistry, Geophysics, Geosystems, v. 4, p. 8.

Conrad, C., and Hager, B., 2001, Mantle convection with strong subduction zones: Geophysical Journal International, v. 144, p. 271–288, doi: 10.1046/j.1365-246x.2001.00321.x.

Cottrell, R., and Tarduno, J., 2000, Late Cretaceous true polar wander: Science, v. 288, p. 2283a.

Dalziel, I., 1991, Pacific margins of Laurentia and East Antarctica–Australia as a conjugate rift pair: Evidence and implications for an Eocambrian supercontinent: Geology, v. 19, p. 598–601, doi: 10.1130/0091-7613(1991)019<0598:PMOLAE>2.3.CO;2.

Darwin, G., 1877, On the influence of geological changes on the Earth's axis of rotation: Philosophical Transactions of the Royal Society of London, v. 167, p. 271–312.

Davis, D., and Green, J., 1997, Geochronology of the North American Midcontinent rift in western Lake Superior and implications for its geodynamic evolution: Canadian Journal of Earth Sciences, v. 34, p. 476–488.

Davis, D., and Paces, J., 1990, Time resolution of geologic events on the Keeweenaw Peninsula and applications for development of the Midcontinent Rift system: Earth and Planetary Science Letters, v. 97, p. 54–64, doi: 10.1016/0012-821X(90)90098-I.

Davis, D., and Sutcliffe, R., 1985, U-Pb ages from the Nipigon plate and northern Lake Superior: Geological Society of America Bulletin, v. 96, p. 1572–1579, doi: 10.1130/0016-7606(1985)96<1572:UAFTNP>2.0.CO;2.

Deblond, A., Punzalan, L., Bowen, A., and Tack, L., 2001, The Malagarazi Supergroup of SE Burundi and its correlative Bukoba Supergroup of NW Tanzania: Neo- and Mesoproterozoic chronostratigraphic constraints from Ar-Ar ages on mafic intrusive rocks: Journal of African Earth Sciences, v. 32, p. 435–449, doi: 10.1016/S0899-5362(01)90107-1.

Dewey, J., and Strachan, R., 2003, Changing Silurian-Devonian relative plate motion in the Caledonides: Sinistral transpression to sinistral transtension: Journal of the Geological Society of London, v. 160, p. 219–229.

Dickens, G., 2001, The potential volume of oceanic methane hydrates: Organic Geochemistry, v. 32, p. 1179–1193, doi: 10.1016/S0146-6380(01)00086-9.

Diehl, J., and Haig, T., 1994, A paleomagnetic study of the lava flows within the Copper Harbour Conglomerate, Michigan: New results and implications: Canadian Journal of Earth Sciences, v. 31, p. 369–380.

DiVenere, V., and Kent, D., 1999, Are the Pacific and Indo-Atlantic hotspots fixed? Testing the plate circuit through Antarctica: Earth and Planetary Science Letters, v. 170, p. 105–117, doi: 10.1016/S0012-821X(99)00096-5.

Donnadieu, Y., Goddéris, Y., Ramstein, G., Nédélec, A., and Meert, J., 2004, A 'snowball Earth' climate triggered by continental break-up through changes in runoff: Nature, v. 428, p. 303–306, doi: 10.1038/nature02408.

Dunlop, D., and Özdemir, Ö., 1997, Rock magnetism: Fundamentals and frontiers: Cambridge, UK, Cambridge University Press, 573 p.

Evans, D., 1998, True polar wander; a supercontinental legacy: Earth and Planetary Science Letters, v. 157, p. 1–8, doi: 10.1016/S0012-821X(98)00031-4.

Evans, D., 2003, True polar wander and supercontinents: Tectonophysics, v. 362, p. 303–320, doi: 10.1016/S0040-1951(02)000642-X.

Evans, D., Ripperdan, R., and Kirschvink, J., 1998, Polar wander and the Cambrian (response): Science, v. 279, p. 9 (correction p. 307).

Evans, D., Li, Z., Kirschvink, J., and Wingate, M., 2000, A high-quality mid-Neoproterozoic paleomagnetic pole from South China, with implications for ice ages and the breakup configuration of Rodinia: Precambrian Research, v. 100, p. 313–334, doi: 10.1016/S0301-9268(99)00079-0.

Fanning, C., and Link, P., 2004, U-Pb SHRIMP age of Neoproterozoic (Sturtian) glaciogenic Pocatello Formation, southeastern Idaho: Geology, v. 35, p. 881–884.

Fanning, C., Ludwig, K., Forbes, B., and Preiss, W., 1986, Single and multiple grain U-Pb zircon analyses for the early Adelaidean Rook Tuff, Willouran Ranges, South Australia: Abstracts of the Geological Society of Australia, v. 15, p. 71–72.

Fisher, D., 1974, Some more remarks on polar wandering: Journal of Geophysical Research, v. 79, p. 4041–4045.

Fisher, R., 1953, Dispersion on a sphere: Proceedings of the Royal Society of London, v. A217, p. 295–305.

Gallet, Y., Pavlov, V., Semikhatov, M., and Petrov, P., 2000, Late Mesoproterozoic magnetostratigraphic results from Siberia: Paleogeographic implications and magnetic field behavior: Journal of Geophysical Research, v. 105, p. 16,481–16,499, doi: 10.1029/1999JB900354.

Gee, D., and Page, L., 1994, Caledonian terrane assembly on Svalbard: New evidence from $^{40}Ar/^{39}Ar$ dating in

Ny Friesland: American Journal of Science, v. 294, p. 1166–1186.

Gee, D., Johansson, Å, Ohta, Y., Tebenkov, A.M., Krasil'schikov, A.A., Balashov, Y.A., Larionov, A.N., Gannibal, L.F., and Ryungenen, G.I., 1995, Grenvillian basement and a major unconformity within the Caledonides of Nordaustlandet, Svalbard: Precambrian Research, v. 70, p. 215–234, doi: 10.1016/0301-9268(94)00041-O.

Gilder, S., Chen, Y., Cogné, J., Tan, X., Courtillot, V., Sun, D., and Li, Y., 2003, Paleomagnetism of Upper Jurassic to Lower Cretaceous volcanic and sedimentary rocks from the western Tarim Basin and implications for inclination shallowing and absolute dating of the M-0 (ISEA?) chron: Earth and Planetary Science Letters, v. 206, p. 587–600, doi: 10.1016/S0012-821X(02)01074-9.

Gold, T., 1955, Instability of the Earth's axis of rotation: Nature, v. 175, p. 526–529.

Goldreich, P., and Toomre, A., 1969, Some remarks on polar wandering: Journal of Geophysical Research, v. 74, p. 2555–2567.

Grotzinger, J., and Knoll, A., 1995, Anomalous carbonate precipitates: Is the Precambrian the key to the Permian?: Palaios, v. 100, p. 578–596.

Gubbins, D., 1999, The distinction between geomagnetic excursions and reversals: Geophysical Journal International, v. 137, p. F1–F3, doi: 10.1046/j.1365-246x.1999.00810.x.

Hager, B., and Clayton, R., 1989, Constraints on the structure of mantle convection using seismic observations, flowmodels, and the geoid: The Fluid Mechanics of Astrophysics and Geophysics, v. 4, p. 657–763.

Halgedahl, S., and Jarrard, R., 1995, Low-temperature behavior of single-domain through multidomain magnetite: Earth and Planetary Science Letters, v. 130, p. 127–139, doi: 10.1016/0012-821X(94)00260-6.

Halls, H., and Pesonen, L., 1982, Paleomagnetism of Keweenawan rocks: Geological Society of America Memoir 156, p. 173–201.

Halverson, G., Maloof, A., and Hoffman, P., 2004, The Marinoan glaciation (Neoproterozoic) in northeast Svalbard: Basin Research, v. 16, p. 297–324, doi: 10.1111/j.1365-2117.2004.00234.x.

Halverson, G., Hoffman, P., Maloof, A., Schrag, D., Rice, A.H.N., Bowring, S., and Dudas, F., 2005, Toward a Neoproterozoic composite carbon-isotope record: Geological Society of America Bulletin, v. 117, p. 1181–1207, doi: 10.1130/B25630.1.

Halverson, G., Maloof, A., Schrag, D., Dudas, F., and Hurtgen, M., 2006, Stratigraphy and geochemistry of a ca. 800 Ma negative carbon isotope stage in northeastern Svalbard: Chemical Geology (in press).

Halvorsen, E., 1989, A paleomagnetic pole position of Late Jurassic/Early Cretaceous dolerites from Hinlopenstretet, Svalbard, and its tectonic implications: Earth and Planetary Science Letters, v. 94, p. 398–408, doi: 10.1016/0012-821X(89)90156-8.

Hanson, R., Crowley, J., Bowring, S., Ramezani, J., Gose, W., Dalziel, I., Pancake, J., Seidel, E., Blenkinsop, T., and Mukwakwami, J., 2004, Coeval large-scale magmatism in the Kalahari and Laurentian cratons during Rodinia assembly: Science, v. 304, p. 1126–1129, doi: 10.1126/science.1096329.

Harlan, S., Geissman, J., and Snee, L., 1997, Paleomagnetic and $^{40}Ar/^{39}Ar$ geochronologic data from Late Proterozoic mafic dykes and sills, Montana and Wyoming: U.S. Geological Survey Professional Paper 1580, 16 p.

Harland, W., 1997, The geology of Svalbard: Geological Society of London Memoir 17, 521 p.

Harland, W., and Gayer, R., 1972, The Arctic Caledonides and earlier oceans: Geological Magazine, v. 109, p. 289–314.

Harland, W., Scott, R., Aukland, K., and Snape, I., 1992, The Ny Friesland orogen, Spitsbergen: Geological Magazine, v. 129, p. 679–708.

Hartz, E., and Torsvik, T., 2002, Baltica upside down: A new plate tectonic model for Rodinia and the Iapetus Ocean: Geology, v. 30, p. 255–258.

Hayes, J., Strauss, H., and Kaufman, A., 2001, Fractionation of the isotopes of carbon and hydrogen in biosynthetic processes, *in* Valley, J., and Cole, D., eds., Geological Society of America Short Course sponsored by the Mineralogical Society of America: Boston, Geological Society of America, p. 1–31.

Heaman, L., LeCheminant, A., and Rainbird, R., 1992, Nature and timing of Franklin igneous events, Canada: Implications for a Late Proterozoic mantle plume and breakup of Laurentia: Earth and Planetary Science Letters, v. 109, p. 117–131, doi: 10.1016/0012-821X(92)90078-A.

Hedges, J., and Keil, R., 1995, Sedimentary organic-matter preservation—An assessment and speculative synthesis: Marine Chemistry, v. 49, p. 81–115, doi: 10.1016/0304-4203(95)00008-F.

Henry, S., Mauk, F., and Van der Voo, R., 1977, Paleomagnetism of the upper Keweenawan sediments: Nonesuch Shale and Freda Sandstone: Canadian Journal of Earth Sciences, v. 14, p. 1128–1138.

Herrington, P., and Fairchild, I., 1989, Carbonate shelf and slope facies evolution prior to Vendian glaciation, central East Greenland, *in* Gayer, R., ed., The Caledonide geology of Scandinavia: London, Graham Trotman, p. 285–297.

Hill, A., and Walter, M., 2000, Mid-Neoproterozoic (~830–750 Ma) isotope stratigraphy of Australia and global correlation: Precambrian Research, v. 100, p. 181–211, doi: 10.1016/S0301-9268(99)00074-1.

Hill, A., Arouri, K., Gorjan, P., and Walter, M., 2000a, Geochemistry of marine and nonmarine environments of a Neoproterozoic cratonic carbonate/evaporite: The Bitter Springs Formation, Central Australia, *in* Grotzinger, J., and James, N., eds., Carbonate sedimentation and diagenesis in an evolving Precambrian world: Tulsa, Society for Sedimentary Geology Special Publication 67, p. 327–344.

Hill, A., Cotter, K., and Grey, K., 2000b, Mid-Neoproterozoic biostratigraphy and isotope stratigraphy in Australia: Precambrian Research, v. 100, p. 281–298, doi: 10.1016/S0301-9268(99)00077-7.

Hoffman, P., 1991, Did the breakout of Laurentia turn Gondwana inside out?: Science, v. 252, p. 1409–1412.

Hoffman, P., Hawkins, D., Isachsen, C., and Bowring, S., 1996, Precise U-Pb zircon ages for early Damaran magmatism in the Summas Mountains and Welwitschia Inlier, northern Damara belt, Namibia: Communications of the Geological Survey of Namibia, v. 11, p. 47–52.

Ingall, E., and Jahnke, R., 1997, Influence of water-column anoxia on the elemental fractionation of carbon and phosphorous during sediment diagenesis: Marine Geology, v. 139, p. 219–229, doi: 10.1016/S0025-3227(96)00112-0.

Ingall, E., and Van Cappellen, P., 1990, Relation between sedimentation rate and burial of organic phosphorous and organic carbon in marine sediments: Geochimica et Cosmochimica Acta, v. 54, p. 373–386, doi: 10.1016/0016-7037(90)90326-G.

Ingall, E., Bustin, R., and Van Cappellen, P., 1993, Influence of water-column anoxia on the burial and preservation of carbon and phosphorous in marine shales: Geochimica et Cosmochimica Acta, v. 57, p. 303–316, doi: 10.1016/0016-7037(93)90433-W.

Ishihara, N., and Kida, S., 2000, Axial and equatorial magnetic dipoles generated in a rotating spheric shell: Journal of the Physical Society of Japan, v. 69, p. 1582–1585, doi: 10.1143/JPSJ.69.1582.

Ishihara, N., and Kida, S., 2002, Equatorial magnetic dipole field intensification by convection vortices in a rotating spherical shell: Fluid Dynamics Research, v. 31, p. 253–274, doi: 10.1016/S0169-5983(02)00118-1.

Jackson, M., 1990, Diagenetic sources of stable remanence in remagnetized Paleozoic cratonic carbonates: A rock magnetic study: Journal of Geophysical Research, v. 95, p. 2753–2761.

Jackson, M., Banerjee, S., Marvin, J., Lu, R., and Gruber, W., 1991, Detrital remanence, inclination errors and anhysteretic remanence anisotropy: Quantitative model and experimental results: Geophysical Journal International, v. 104, p. 95–103.

Jackson, M., Sun, W.-W., and Craddock, J., 1992, The rock magnetic fingerprint of chemical remagnetization in midcontinental Paleozoic carbonates: Geophysical Research Letters, v. 19, p. 781–784.

Jelénska, M., 1987, Aspects of pre-Tertiary paleomagnetism of Spitsbergen and their tectonic implications: Tectonophysics, v. 139, p. 99–106, doi: 10.1016/0040-1951(87)90199-5.

Jelénska, M., and Lewandowski, M., 1986, A palaeomagnetic study of Devonian sandstone from central Spitsbergen: Geophysical Journal of the Royal Astronomical Society, v. 87, p. 617–632.

Jelénska, M., and Vincenz, S., 1987, Origin of the magnetization of Permo-Carboniferous sediments of Spitsbergen, Svalbard Archipelago: Earth and Planetary Science Letters, v. 85, p. 173–182, doi: 10.1016/0012-821X(87)90030-6.

Jiang, G., Sohl, L., and Christie-Blick, N., 2003, Neoproterozoic stratigraphic comparison of the Lesser Himalaya (India) and Yangtze block (south China): Paleogeographic implications: Geology, v. 31, p. 917–920, doi: 10.1130/G19790.1.

Johannson, Å., Larianov, A., Tebenkov, A., Gee, D., Whitehouse, M., and Vestin, J., 2001, Grenvillian magmatism of western and central Nordaustlandet, northeastern Svalbard: Transactions of the Royal Society of Edinburgh, v. 90, p. 221–234.

Jones, C., and Tetreault, J., 2004, PaleoMag OS X: http://cires.colorado.edu/people/jones.craig/PMag3.html (last accessed May 2006).

Jones, D., Bates, M., Li, Z., Corner, B., and Hodgkinson, G., 2003, Paleomagnetic results from the ca. 1130 Ma Borgmassivet intrusions in the Ahlmannryggen region of Dronning Maud Land, Antarctica, and tectonic implications: Tectonophysics, v. 375, p. 247–260, doi: 10.1016/S0040-1951(03)00341-X.

Junge, C., Schidlowski, M., Eichmann, R., and Pietrek, H., 1975, Model calculations for the terrestrial carbon cycle: Carbon isotope geochemistry and evolution of photosynthetic oxygen: Journal of Geophysical Research, v. 80, p. 4542–4552.

Jurdy, D., and Van der Voo, R., 1974, A method for the separation of true polar wander and continental drift, including results for the last 55 m.y.: Journal of Geophysical Research, v. 79, p. 2945–2952.

Jurdy, D., and Van der Voo, R., 1975, True polar wander since the Early Cretaceous: Science, v. 187, p. 1193–1196.

Karlstrom, K., Harlan, S., Williams, M., McLelland, J., Geissman, J., and Åhäll, K.-I., 1999, Refining Rodinia: Geologic evidence for the Australia–Western U.S. connection in the Proterozoic: GSA Today, v. 9, no. 10, p. 1–7.

Keil, R.G., Montluçon, D.B., Prahl, F.G., and Hedges, J.I., 1994, Sorptive preservation of labile organic matter in marine sediments: Nature, v. 370, p. 549–552.

Kent, D., and Smethurst, M., 1998, Shallow bias of paleomagnetic inclinations in the Paleozoic and Precambrian: Earth and Planetary Science Letters, v. 160, p. 391–402, doi: 10.1016/S0012-821X(98)00099-5.

Kim, B.Y., and Kodama, K.P., 2004, A compaction correction for paleomagnetism of the Nanaimo group sedimentary rocks: Implications for the Baja British Columbia hypothesis: Journal of Geophysical Research, v. 109, no. B2, B02102, doi: 10.1029/2003JB002696.

Kirschvink, J., 1980, The least-squares line and plane and the analysis of paleomagnetic data: Geophysical Journal of the Royal Astronomical Society, v. 62, p. 699–718.

Kirschvink, J., 2002, A new automated sample changer: Eos (Transactions, American Geophysical Union), v. 83, p. S324.

Kirschvink, J., and Raub, T., 2003, A methane fuse for the Cambrian explosion: Carbon cycles and true polar wander: Comptes Rendues Geoscience, v. 335, p. 65–78, doi: 10.1016/S1631-0713(03)00011-7.

Kirschvink, J., Ripperdan, R., and Evans, D., 1997, Evidence of a large-scale reorganization of Early Cambrian continental masses by inertial interchange true polar wander: Science, v. 277, p. 541–545, doi: 10.1126/science.277.5325.541.

Knoll, A., and Swett, K., 1990, Carbonate deposition during the Late Proterozoic era: An example from Spitsbergen: American Journal of Science, v. 290, p. 104–132.

Knoll, A., Hayes, J., Kaufman, A., Swett, K., and Lambert, I., 1986, Secular variation in carbon isotope ratios from Upper Proterozoic successions of Svalbard and east Greenland: Nature, v. 321, p. 832–837, doi: 10.1038/321832a0.

Kodama, K., and Sun, W., 1992, Magnetic anisotropy as a correction for compaction-caused paleomagnetic incli-

nation shallowing: Geophysical Journal International, v. 111, p. 465–469.
Kump, L.R., 1988, Terrestrial feedback in atmospheric oxygen regulation by fire and phosphorus: Nature, v. 335, p. 152–154, doi: 10.1038/335152a0.
Kump, L.R., 1991, Interpreting carbon-isotopic excursions: Strangelove oceans: Geology, v. 19, p. 299–302, doi: 10.1130/0091-7613(1991)019<0299:ICIESO>2.3.CO;2.
Kutzner, C., and Christensen, U., 2000, Effects of driving mechanisms in geodynamo models: Geophysical Research Letters, v. 27, p. 29–32, doi: 10.1029/1999GL010937.
Kvenvolden, K., 1999, Potential effects of gas hydrate on human welfare: Proceedings of the National Academy of Sciences of the United States of America, v. 96, p. 3420–3426, doi: 10.1073/pnas.96.7.3420.
Lallemand, S., Heuret, A., and Boutelier, D., 2005, On the relationships between slab dip, backarc stress, upper plate absolute motion, and crustal nature in subduction zones: Geochemistry, Geophysics, Geosystems, v. 6, doi: 10.1029/2005GC000917.
Langereis, C., Dekkers, M., de Lange, G., Paterne, M., and van Santvoort, P., 1997, Magnetostratigraphy and astronomical calibration of the last 1.1 Myr from an eastern Mediterranean piston core and dating of short events in the Brunhes: Geophysical Journal International, v. 129, p. 75–94.
LeCheminant, A., and Heaman, L., 1994, 779 Ma mafic magmatism in the northwestern Canadian Shield and northern Cordillera: A new regional time-marker: Proceedings of the 8th International Conference: Geochronology, Cosmochronology and Isotope Geology, Program Abstracts, v. 1107, p. 197.
Lenton, T., and Watson, A., 2000, Redfield revisited: 1. Regulation of nitrate, phosphate, and oxygen in the ocean: Global Biogeochemical Cycles, v. 14, p. 225–248, doi: 10.1029/1999GB900065.
LePichon, X., and Sibuet, J.-C., 1981, Passive margins: A model of formation: Journal of Geophysical Research, v. 86, p. 3708–3720.
Li, Z., 2000, New paleomagnetic results from the 'cap dolomite' of the Neoproterozoic Walsh Tillite, northwestern Australia: Precambrian Research, v. 100, p. 359–370, doi: 10.1016/S0301-9268(99)00081-9.
Li, Z., Evans, D., and Zhang, S., 2004, A 90° spin on Rodinia: Possible causal links between the Neoproterozoic supercontinent, superplume, true polar wander and low-latitude glaciation: Earth and Planetary Science Letters, v. 220, p. 409–421, doi: 10.1016/S0012-821X(04)00064-0.
Lister, D., and Buffet, B., 1995, The strength and efficiency of thermal and compositional convection in the geodynamo: Physics of the Earth and Planetary Interiors, v. 91, p. 17–30, doi: 10.1016/0031-9201(95)03042-U.
Livermore, R., Vine, F., and Smith, A., 1984, Plate motions and the geomagnetic field: II. Jurassic to Tertiary: Geophysical Journal of the Royal Astronomical Society, v. 79, p. 939–961.
Long, D., 1989, Ella Bay Formation: Early Cambrian shelf differentiation in the Franklinian Basin, central eastern Ellesmere Island, Arctic Canada: Canadian Journal of Earth Sciences, v. 26, p. 2621–2635.
Løvlie, R., Torsvik, T., Jelénska, M., and Lewandowski, M., 1984, Evidence for detritral remanent magnetization carried by hematite in Devonian red beds from Spitsbergen; Palaeomagnetic implications: Geophysical Journal of the Royal Astronomical Society, v. 79, p. 573–588.
Lyberis, N., and Manby, G., 1999, Continental collision and lateral escape deformation in the lower upper crust: An example from the Caledonides of Svalbard: Tectonics, v. 18, p. 40–63, doi: 10.1029/1998TC900013.
Maloof, A., Grotzinger, J., Kopp, R., Weiss, B., Vali, H., and Kirschvink, J., 2005, On the origin of magnetization in platformal carbonate muds: Eos (Transactions, American Geophysical Union), Fall Meeting Supplement, v. 86, p. B24A–07.
Marcano, M., Van der Voo, R., and MacNiocaill, C., 1999, True polar wander during the Permo-Triassic: Geodynamics, v. 28, p. 75–95, doi: 10.1016/S0264-3707(98)00026-X.
Martin, A., Nisbet, E., Bickle, M., and Orpen, J., 1993, Rock units and stratigraphy of the Belingwe greenstone belt: The complexity of the tectonic setting, *in* Bickle, M., and Nisbet, E., eds., The geology of the Belingwe greenstone belt, Zimbabwe: Geological Society of Zimbabwe Special Publication 2, p. 39–68.
Martin, D.M., Clendenin, C., Krapez, B., and McNaughton, N., 1998, Tectonic and geochronological constraints on Late Archaean and Palaeoproterozoic stratigraphic correlation with and between the Kaapvaal and Pilbara cratons: Journal of the Geological Society of London, v. 155, p. 311–322.
Matsuyama, I., Mitrovica, J., Manga, M., Perron, J., and Richards, M., 2006, Rotational stability of dynamic planets with elastic lithospheres: Journal of Geophysical Research, v. 111, E02003, doi: 10.1029/2005JE002447.
Mayer, L., 1999, Extent of coverage of mineral surfaces by organic matter in marine sediments: Geochimica et Cosmochimica Acta, v. 63, p. 207–215, doi: 10.1016/S0016-7037(99)00028-9.
McCabe, C., and Elmore, R., 1989, The occurrence and origin of late Paleozoic remagnetization in the sedimentary rocks of North America: Reviews of Geophysics, v. 27, p. 471–494.
McCabe, C., and Van der Voo, R., 1983, Paleomagnetic results from the Upper Keweenawan Chequamegon Sandstone: Implications for red bed diagenesis and Late Precambrian apparent polar wander of North America: Canadian Journal of Earth Sciences, v. 20, p. 105–112.
McCabe, C., Van der Voo, R., Peacor, D., Scotese, C., and Freeman, R., 1983, Diagenetic magnetite carries ancient yet secondary remanence in some Paleozoic sedimentary carbonates: Geology, v. 11, p. 221–223, doi: 10.1130/0091-7613(1983)11<221:DMCAYS>2.0.CO;2.
McCabe, C., Jackson, M., and Saffer, B., 1989, Regional patterns of magnetite authigenesis in the Appalachian Basin: Implications for the mechanism of late Paleozoic remagnetization: Journal of Geophysical Research, v. 94, p. 10,429–10,443.
McElhinny, M., 1964, Statistical significance of the fold test in paleomagnetism: Royal Astronomical Society Geophysical Journal, v. 80, p. 338–340.
McElhinny, M., 1973, Mantle plumes, palaeomagnetism, and polar wandering: Nature, v. 241, p. 523–524, doi: 10.1038/241523a0.
McElhinny, M., and McFadden, P., 2000, Paleomagnetism: Continents and oceans: San Diego, Academic Press, International Geophysics Series, v. 73, 386 p.
McFadden, P., 1998, The fold test as an analytical tool: Geophysical Journal International, v. 135, p. 329–338, doi: 10.1046/j.1365-246X.1998.00640.x.
McFadden, P., and Jones, D., 1981, The fold test in paleomagnetism: Royal Astronomical Society Geophysical Journal, v. 67, p. 53–58.
McFadden, P., and McElhinny, M., 1988, The combined analysis of remagnetization circles and direct observations in paleomagnetism: Earth and Planetary Science Letters, v. 87, p. 161–172, doi: 10.1016/0012-821X(88)90072-6.
McFadden, P., and McElhinny, M., 1990, Classification of the reversals test in palaeomagnetism: Geophysical Journal International, v. 103, p. 725–729.
McKenzie, D., 1972, Plate tectonics, *in* Robertson, E., ed., The nature of the solid Earth: New York, McGraw-Hill, p. 323–360.
McKenzie, D., 1978, Some remarks on the development of sedimentary basins: Earth and Planetary Science Letters, v. 40, p. 25–32, doi: 10.1016/0012-821X(78)90071-7.
McNeill, D., 1997, Facies and early diagenetic influence on the depositional magnetization of carbonates: Geology, v. 25, p. 799–802, doi: 10.1130/0091-7613(1997)025<0799:FAEDIO>2.3.CO;2.
McNeill, D., and Kirschvink, J., 1993, Early dolomitization of platform carbonates and the preservation of magnetic polarity: Journal of Geophysical Research, v. 98, p. 7977–7986.
McWilliams, M., and McElhinny, M., 1980, Late Precambrian paleomagnetism of Australia: The Adelaide geosyncline: The Journal of Geology, v. 80, p. 1–26.
Meert, J., 1999, A paleomagnetic analysis of Cambrian true polar wander: Earth and Planetary Science Letters, v. 168, p. 131–144, doi: 10.1016/S0012-821X(99)00042-4.
Meert, J., Van der Voo, R., and Ayub, S., 1995, Paleomagnetic investigation of the Neoproterozoic Gagwe lavas and Mbozi complex, Tanzania, and the assembly of Gondwana: Precambrian Research, v. 74, p. 225–244, doi: 10.1016/0301-9268(95)00012-T.
Meert, J., Van der Voo, R., Pisarevsky, S., Komissarova, R., and Khramov, A., 2001, New palaeomagnetic results from Vendian red sediments in Cisbaikalia and the problem of the relationship of Siberia and Laurentia in the Vendian; discussion and reply: Geophysical Journal International, v. 146, p. 867–873, doi: 10.1046/j.0956-540x.2001.01474.x.
Merrill, R., McElhinny, M., and McFadden, P., 1998, The magnetic field of the Earth: San Diego, Academic Press, International Geophysics Series, v. 63, 531 p.
Mertanen, S., Pesonen, L., and Huhma, H., 1996, Paleomagnetism and Sm-Nd ages of the Neoproterozoic diabase dykes in Laanila and Kautokeino, northern Fennoscandia, *in* Brewer, T., ed., Precambrian crustal evolution in the North Atlantic region: Geological Society [London] Special Publication 112, p. 331–358.
Miller, J., and Kent, D., 1988, Regional trends in the timing of Alleghenian remagnetization in the Appalachians: Geology, v. 16, p. 588–591, doi: 10.1130/0091-7613(1988)016<0588:RTITTO>2.3.CO;2.
Miller, K., and Hargraves, R., 1994, Paleomagnetism of some Indian kimberlites and lamproites: Precambrian Research, v. 69, p. 259–267, doi: 10.1016/0301-9268(94)90090-6.
Mitrovica, J.X., Wahr, J., Matsuyama, I., and Paulson, A., 2005, The rotational stability of an ice-age earth: Geophysical Journal International, v. 161, p. 491–506.
Möller, C., and Söderlund, U., 1997, Age constraints on the deformation within the Eastern Segment SW Sweden: Late Sveconorwegian granite dyke intrusion and metamorphic-deformational relations: Geologiska Föreningen i Stockholm Förhandlingar, v. 119, p. 1–12.
Morgan, W., 1981, Hotspot tracks and the opening of the Atlantic and Indian Oceans, *in* Emiliani, C., ed., The Sea 7: New York, John Wiley and Sons, v. 13, p. 443–487.
Moskowitz, B., Frankel, R., Flanders, P., Blakemore, R., and Schwartz, B., 1988, Magnetic properties of magnetotactic bacteria: Journal of Magnetism and Magnetic Materials, v. 73, p. 273–288, doi: 10.1016/0304-8853(88)90093-5.
Moskowitz, B., Frankel, R., and Bazylinski, D., 1993, Rock magnetic criteria for the detection of biogenic magnetite: Earth and Planetary Science Letters, v. 120, p. 283–300, doi: 10.1016/0012-821X(93)90245-5.
Moskowitz, B., Jackson, M., and Kissel, C., 1998, Low-temperature magnetic behavior of titanomagnetites: Earth and Planetary Science Letters, v. 157, p. 141–149, doi: 10.1016/S0012-821X(98)00033-8.
Mound, J., and Mitrovica, J., 1998, True polar wander as a mechanism for second-order sea-level variations: Science, v. 279, p. 534–537, doi: 10.1126/science.279.5350.534.
Mound, J., Mitrovica, J., Evans, D., and Kirschvink, J., 1999, A sea-level test for inertial interchange true polar wander events: Geophysical Journal International, v. 136, p. F5–F10, doi: 10.1046/j.1365-246x.1999.00791.x.
Mound, J., Mitrovica, J., and Milne, G., 2001, Sea-level and true polar wander during the Late Cretaceous: Geophysical Research Letters, v. 28, p. 2057–2060, doi: 10.1029/2000GL012369.
Mound, J., Mitrovica, J., and Forte, A., 2003, The equilibrium form of a rotating Earth with an elastic shell: Geophysical Journal International, v. 152, p. 237–241, doi: 10.1046/j.1365-246X.2003.01857.x.
Nakiboglu, S., and Lambeck, K., 1980, Deglaciation effects on the rotation of the Earth: Geophysical Journal of the Royal Astronomical Society, v. 62, p. 49–58.
Nawrocki, J., 1999, Paleomagnetism of Permian through Early Triassic sequences in central Spitsbergen: Implications for paleogeography: Earth and Planetary Science Letters, v. 169, p. 59–70, doi: 10.1016/S0012-821X(99)00069-2.
Norin, E., 1937, Reports from the Scientific Expedition to the Northwestern Provinces of China under the Leadership of Dr. Sven Hedin, III, Bokförlags Aktiebolaget Thule, Stockholm, chap. 1, Geology: Eastern Tien-Shan, Geology of Western Quruqtagh: Stockholm, Bokförlags Aktiebolaget Thule, 194 p.
Oliver, J., 1986, Fluids expelled tectonically from orogenic belts: Their role in hydrocarbon migration and other

geologic phenomena: Geology, v. 14, p. 99–102, doi: 10.1130/0091-7613(1986)14<99:FETFOB>2.0.CO;2.

Özdemir, Ö., and Dunlop, D., 2003, Low-temperature behavior and memory of iron-rich titanomagnetites (Mt. Haruna, Japan and Mt. Pinatubo, Philippines): Earth and Planetary Science Letters, v. 216, p. 193–200, doi: 10.1016/S0012-821X(03)00481-3.

Park, J., 1994, Paleomagnetic constraints on the position of Laurentia from middle Neoproterozoic to Early Cambrian times: Precambrian Research, v. 69, p. 95–112, doi: 10.1016/0301-9268(94)90081-7.

Park, J., Norris, D., and LaRochelle, A., 1989, Paleomagnetism and the origin of the Mackenzie Arc of northwestern Canada: Canadian Journal of Earth Sciences, v. 26, p. 2194–2203.

Peltier, W., 1998, Postglacial variations in the level of the sea: Implications for climate dynamics and solid-Earth geophysics: Reviews of Geophysics, v. 36, p. 603–689, doi: 10.1029/98RG02638.

Piper, J., 2000, The Neoproterozoic supercontinent: Rodinia or Paleopangaea: Earth and Planetary Science Letters, v. 176, p. 131–146, doi: 10.1016/S0012-821X(99)00314-3.

Pisarevsky, S., and Bylund, G., 1998, Paleomagnetism of a key section of the Protogine zone, southern Sweden: Geophysical Journal International, v. 133, p. 185–200, doi: 10.1046/j.1365-246X.1998.1331497.x.

Pisarevsky, S., Komissarova, R., and Khramov, A., 2000, New paleomagnetic results from Vendian red sediments in Cisbaikalia and the problem of the relationship of Siberia and Laurentia in the Vendian: Geophysical Journal International, v. 140, p. 598–610, doi: 10.1046/j.1365-246X.2000.t01-1-00056.x.

Pisarevsky, S., Wingate, T., Powell, C.M., Johnson, S., and Evans, D., 2003, Models of Rodinia assembly and fragmentation, *in* Yoshida, M., Windley, B., and Dasgupta, S., eds., Proterozoic East Gondwana: Supercontinent assembly and breakup: Geological Society [London] Special Publication 206, p. 35–55.

Powell, C., Jones, D., Pisarevsky, S., and Wingate, M., 2001, Paleomagnetic constraints on the position of the Kalahari craton in Rodinia: Precambrian Research, v. 110, p. 33–46, doi: 10.1016/S0301-9268(01)00179-6.

Preiss, W., 2000, The Adelaide geosyncline of South Australia and its significance in Neoproterozoic continental reconstruction: Precambrian Research, v. 100, p. 21–63, doi: 10.1016/S0301-9268(99)00068-6.

Prévot, M., Mattern, E., Camps, P., and Daignieres, M., 2000, Evidence for a 20° tilting of the Earth's rotation axis 110 million years ago: Earth and Planetary Science Letters, v. 179, p. 517–528, doi: 10.1016/S0012-821X(00)00129-1.

Radhakrishna, T., and Mathew, J., 1996, Late Precambrian (850–800 Ma) palaeomagnetic pole for the south Indian Shield from the Harohalli alkaline dykes: Geotectonic implications for Gondwana reconstructions: Precambrian Research, v. 80, p. 77–87, doi: 10.1016/S0301-9268(96)00006-X.

Rainbird, R., Jefferson, C., and Young, G., 1996, The early Neoproterozoic sedimentary Succession B of northwestern Laurentia: Correlations and paleogeographic significance: Geological Society of America Bulletin, v. 108, p. 454–470, doi: 10.1130/0016-7606(1996)108<0454:TENSSB>2.3.CO;2.

Ranalli, G., 1995, Rheology of the Earth: London, Chapman and Hall, 413 p.

Ricard, Y., Spada, G., and Sabadini, R., 1993, Polar wandering of a dynamic Earth: Geophysical Journal International, v. 113, p. 284–298.

Richards, M., and Hager, B., 1984, Geoid anomalies in a dynamic Earth: Journal of Geophysical Research, v. 89, p. 5987–6002.

Richards, M., Ricard, Y., Lithgow-Bertelloni, C., Spada, G., and Sabadini, R., 1997, An explanation for Earth's long-term rotational stability: Science, v. 275, p. 372–375, doi: 10.1126/science.275.5298.372.

Rivers, T., 1997, Lithotectonic elements of the Grenville Province: Review and tectonic implications: Precambrian Research, v. 86, p. 117–154, doi: 10.1016/S0301-9268(97)00038-7.

Rocchia, R., Bonte, P., Jehanno, C., Boclet, D., and Chen, Y., 1990, The Cretaceous-Tertiary boundary at Gubbio revisited—Vertical extent of the Ir anomaly: Earth and Planetary Science Letters, v. 99, p. 206–219, doi: 10.1016/0012-821X(90)90111-A.

Rothman, D., Hayes, J., and Summons, R., 2003, Dynamics of the Neoproterozoic carbon cycle: Proceedings of the National Academy of Sciences of the United States of America, v. 100, p. 8124–8129, doi: 10.1073/pnas.0832439100.

Roy, J., and Robertson, W., 1978, Paleomagnetism of the Jacobsville Formation and the apparent polar wander path for the interval ~1100 to ~670 m.y. for North America: Journal of Geophysical Research, v. 83, p. 1289–1304.

Sabadini, R., and Peltier, W., 1981, Pleistocene deglaciation and the Earth's rotation: Implications for mantle viscosity: Geophysical Journal of the Royal Astronomical Society, v. 66, p. 553–578.

Sabadini, R., and Yuen, D., 1989, Mantle stratification and long-term polar wander: Nature, v. 339, p. 373–375, doi: 10.1038/339373a0.

Sabadini, R., Yuen, D., and Boschi, E., 1982, Polar wandering and the forced responses of a rotating, multilayered, viscoelastic planet: Journal of Geophysical Research, v. 87, p. 2885–2903.

Sabadini, R., Doglioni, C., and Yuen, D., 1990, Eustatic sea level fluctuations induced by polar wander: Nature, v. 345, p. 708–710, doi: 10.1038/345708a0.

Sager, W., and Koppers, A., 2000, Late Cretaceous polar wander of the Pacific plate: Evidence of a rapid true polar wander event: Science, v. 287, p. 455–459, doi: 10.1126/science.287.5452.455.

Schneider, D., and Kent, D., 1986, Influence of non-dipole field on determination of Plio-Pleistocene true polar wander: Geophysical Research Letters, v. 13, p. 471–474.

Schrag, D., Berner, R., Hoffman, P., and Halverson, G., 2002, On the initiation of a snowball Earth: Geochemistry, Geophysics, Geosystems, v. 300, doi: 10.1029/2001GC000219.

Sears, J., and Price, R., 2000, New look at the Siberian connection: No SWEAT: Geology, v. 28, p. 423–426, doi: 10.1130/0091-7613(2000)028<0423:NLATSC>2.3.CO;2.

Smith, S., 1984, Phosphorous versus nitrogen limitation in the marine environment: Limnology and Oceanography, v. 29, p. 1149–1160.

South African Committee for Stratigraphy, 1980, Stratigraphy of South Africa, Part 1, *in* Kent, L.E., compiler, Lithostratigraphy of the Republic of South Africa, South West Africa/Namibia, and the Republics of Bohuthatswana, Transkei and Venda: Pretoria, Handbook 8 of the Geological Survey of South Africa, p. 690.

Southgate, P., 1989, Relationships between cyclicity and stromatolite form in the Late Proterozoic Bitter Springs Formation, Australia: Sedimentology, v. 36, p. 323–339.

Spada, G., Ricard, Y., and Sabadini, R., 1992, Excitation of true polar wander by subduction: Nature, v. 360, p. 452–454, doi: 10.1038/360452a0.

Spall, H., 1968, Anomalous paleomagnetic poles from Late Mesozoic dolerites from Spitsbergen: Earth and Planetary Science Letters, v. 4, p. 73–78, doi: 10.1016/0012-821X(68)90057-5.

Stacey, F., 1992, Physics of the Earth (third edition): Brisbane, Australia, Brookfield Press, 513 p.

Stearn, J., and Piper, J., 1984, Palaeomagnetism of the Sveconorwegian mobile belt of the Fennoscandian Shield: Precambrian Research, v. 23, p. 201–246, doi: 10.1016/0301-9268(84)90045-7.

Steinberger, B., and O'Connell, R., 1997, Changes of the Earth's rotation axis owing to advection of mantle density heterogeneities: Nature, v. 387, p. 169–173, doi: 10.1038/387169a0.

Steinberger, B., and O'Connell, R., 1998, Advection of plumes in mantle flow: Implications for hotspot motion, mantle viscosity and plume distribution: Geophysical Journal International, v. 132, p. 412–434, doi: 10.1046/j.1365-246x.1998.00447.x.

Steinberger, B., and O'Connell, R., 2002, The convective mantle flow signal in rates of true polar wander, *in* Mitrovica, J.X., and Vermeersen, L.L.A., eds., Ice Sheets, Sea Level and the Dynamic Earth: American Geophysical Union, Geodynamics Series 29, v. 29, p. 233–256.

Steinberger, B., Sutherland, R., and O'Connell, R., 2004, Prediction of Emperor-Hawaii seamount locations from a revised model of global plate motion and mantle flow: Nature, v. 430, p. 167–173, doi: 10.1038/nature02660.

Stolz, J., Chang, S.R., and Kirschvink, J., 1986, Magnetotactic bacteria and single-domain magnetite in hemipelagic sediments: Nature, v. 321, p. 849–851, doi: 10.1038/321849a0.

Strik, G., Blake, T., Zegers, T., White, S., and Langereis, C., 2003, Palaeomagnetism of flood basalts in the Pilbara craton, Western Australia: Late Archean continental drift and the oldest known reversal of the geomagnetic field: Journal of Geophysical Research, v. 108, p. 2551, doi: 10.1029/2003JB002475.

Surlyk, F., 1991, Tectonostratigraphy of North Greenland: Bulletin Grønlands Geologiske Undersøgelse, v. 160, p. 25–47.

Svenningsen, O., 2001, Onset of seafloor spreading in the Iapetus Ocean at 608 Ma: Precise age of the Sarek Dyke Swarm, northern Swedish Caledonides: Precambrian Research, v. 110, p. 241–254, doi: 10.1016/S0301-9268(01)00189-9.

Tan, X., and Kodama, K.P., 1998, Compaction-corrected inclinations from southern California Cretaceous marine sedimentary rocks indicate no paleolatitudinal offset for the Peninsular Ranges terrane: Journal of Geophysical Research, v. 103, p. 27,169–27,192, doi: 10.1029/98JB02343.

Tan, X., Kodama, K., Chen, H., Fang, D., Sun, D., and Li, Y., 2003, Paleomagnetism and magnetic anisotropy of Cretaceous red beds from the Tarim Basin northwest China: Evidence for a rock magnetic cause of anomalously shallow paleomagnetic inclinations from Central Asia: Journal of Geophysical Research, v. 108, 2107, doi: 10.1029/2001JB001608.

Tarduno, J., and Cottrell, R., 1997, Paleomagnetic evidence for motion of the Hawaiian hotspot during formation of the Emperor seamounts: Earth and Planetary Science Letters, v. 153, p. 171–180, doi: 10.1016/S0012-821X(97)00169-6.

Tarduno, J., and Gee, J., 1995, Large scale motion between Pacific and Atlantic hotspots: Nature, v. 378, p. 477–480, doi: 10.1038/378477a0.

Tauxe, L., and Kent, D., 1984, Properties of a detrital remanence carried by hematite from study of modern river deposits and laboratory redeposition experiments: Geophysical Journal of the Royal Astronomical Society, v. 77, p. 543–561.

Tauxe, L., Bertram, H., and Seberino, C., 2002, Physical interpretation of hysteresis loops: Micromagnetic modeling of fine particle magnetite: Geochemistry, Geophysics, Geosystems, v. 37, p. 1–22.

Tohver, E., van der Pluijm, B., Van der Voo, R., Rizzotto, G., and Scandolara, J., 2002, Paleogeography of the Amazon craton at 1.2 Ga: Early Grenvillian collision with the Llano segment of Laurentia: Earth and Planetary Science Letters, v. 199, p. 185–200, doi: 10.1016/S0012-821X(02)00561-7.

Torsvik, T., and Eide, E., 1997, Database of Norwegian geochronology: Norges Geologiske Undersøkelse Report, v. 98–003.

Torsvik, T., and Rehnström, E., 2001, Cambrian palaeomagnetic data from Baltica: Implications for true polar wander and Cambrian palaeogeography: Journal of the Geological Society of London, v. 158, p. 321–329.

Torsvik, T., and Rehnström, E., 2003, The Rodinia jigsaw puzzle: Science, v. 300, p. 1379–1381, doi: 10.1126/science.1083469.

Torsvik, T., Smethurst, M., Meert, J., Van der Voo, R., McKerrow, W., Brasier, M., Sturt, B., and Walderhaug, H., 1996, Continental break-up and collision in the Neoproterozoic and Paleozoic—Tale of Baltica and Laurentia: Earth-Science Reviews, v. 40, p. 229–258, doi: 10.1016/0012-8252(96)00008-6.

Torsvik, T., Meert, J., and Smethurst, M., 1998, Polar wander and the Cambrian: Science, v. 279, p. 9 (correction p. 307).

Torsvik, T., Ashwal, L., Tucker, R., and Eide, E., 2001a, Neoproterozoic geochronology and palaeogeography of the Seychelles microcontinent: The India link: Precambrian Research, v. 110, p. 47–59, doi: 10.1016/S0301-9268(01)00180-2.

Torsvik, T., Carter, L., Ashwal, L., Bhushan, S., Pandit, M., and Jamtveit, B., 2001b, Rodinia refined or obscured: Palaeomagnetism of the Malani igneous suite (NW

India): Precambrian Research, v. 108, p. 319–333, doi: 10.1016/S0301-9268(01)00139-5.
Tyrrell, T., 1999, The relative influences of nitrogen and phosphorous on oceanic primary production: Nature, v. 400, p. 525–531, doi: 10.1038/22941.
Uno, K., and Bice, D., 2001, Upper Cretaceous paleomagnetism from Umbria, Italy: "Anchored" poles set proposed true polar wander event adrift: Washington, D.C., American Geophysical Union, Spring Meeting, Abstract T51A-08.
Vali, H., and Kirschvink, J., 1989, Magnetofossil dissolution in a palaeomagnetically unstable deep sea sediment: Nature, v. 339, p. 203–206, doi: 10.1038/339203a0.
Van Cappellen, P., and Ingall, E., 1996, Redox stabilization of the atmosphere and oceans by phosphorous-limited marine productivity: Science, v. 271, p. 493–496.
Van der Voo, R., 1989, Paleomagnetism of continental North America: The craton, its margins, and the Appalachian belt, *in* Pakiser, L., and Mooney, W., eds., Geophysical framework of the continental United States: Geological Society of America Memoir 172, p. 447–470.
Van der Voo, R., 1990, The reliability of paleomagnetic data: Tectonophysics, v. 184, p. 1–9, doi: 10.1016/0040-1951(90)90116-P.
Van der Voo, R., 1993, Paleomagnetism of the Atlantic, Tethys and Iapetus Oceans: Cambridge, UK, Cambridge University Press, 411 p.
Van der Voo, R., 1994, True polar wander during the middle Paleozoic: Earth and Planetary Science Letters, v. 122, p. 239–243, doi: 10.1016/0012-821X(94)90063-9.
Van der Westhuizen, W.A., De Bruyn, H., and Meintjes, P.G., 1991, The Ventersdorp Supergroup: An overview: Journal of African Earth Sciences, v. 13, p. 83–105.
Vermeersen, L., and Sabadini, R., 1999, Polar wander, sea-level variations and ice age cycles: Surveys in Geophysics, v. 20, p. 415–440, doi: 10.1023/A:1006691724099.
Walderhaug, H., Torsvik, T., Eide, E., Sundvoll, E., and Bingen, B., 1999, Geochronology and palaeomagnetism of the Hunnedalen dykes, SW Norway: Implications for the Sveconorwegian apparent polar wander loop: Earth and Planetary Science Letters, v. 169, p. 71–83, doi: 10.1016/S0012-821X(99)00066-7.
Watts, D., 1985, Palaeomagnetism of the Lower Carboniferous Billefjorden Group, Spitsbergen: Geological Magazine, v. 122, p. 383–388.
Weil, A., Van der Voo, R., Mac Niocaill, C., and Meert, J., 1998, The Proterozoic supercontinent Rodinia: Paleomagnetically derived reconstructions for 1100 to 800 Ma: Earth and Planetary Science Letters, v. 154, p. 13–24, doi: 10.1016/S0012-821X(97)00127-1.
Weiss, B., Kim, S., Kirschvink, J., Kopp, R., Sankaran, M., Kobayashi, A., and Komeili, A., 2004, Ferromagnetic resonance and low-temperature magnetic tests for biogenic magnetite: Earth and Planetary Science Letters, v. 224, p. 73–89, doi: 10.1016/j.epsl.2004.04.024.
Willemann, R., 1984, Reorientation of planets with elastic lithospheres: Icarus, v. 60, p. 701–709, doi: 10.1016/0019-1035(84)90174-X.
Wingate, M., 2001, SHRIMP baddeleyite and zircon ages for an Umkondo dolerite sill, Nyanga Mountains, eastern Zimbabwe: South African Journal of Geology, v. 104, p. 13–22, doi: 10.2113/104.1.13.
Wingate, M., and Giddings, J., 2000, Age and paleomagnetism of the Mundine Well dyke swarm, Western Australia: Implications for an Australian-Laurentia connection at 755 Ma: Precambrian Research, v. 100, p. 335–357, doi: 10.1016/S0301-9268(99)00080-7.
Wingate, M., Pisarevsky, S., and Evans, D., 2002, A revised Rodinia supercontinent: No SWEAT, no AUSWUS: Terra Nova, v. 14, p. 121–128, doi: 10.1046/j.1365-3121.2002.00401.x.
Wu, P., and Peltier, W., 1984, Pleistocene deglaciation and the Earth's rotation: A new analysis: Geophysical Journal of the Royal Astronomical Society, v. 76, p. 753–791.
Xiao, S., Bao, H., Wang, H., Kaufman, A., Zhou, C., Li, G., Yuan, X., and Ling, H., 2004, The Neoproterozoic Quruqtagh Group in eastern Chinese Tianshan: Evidence for a post-Marinoan glaciation: Precambrian Research, v. 130, p. 1–26, doi: 10.1016/j.precamres.2003.10.013.
Zijderveld, J., 1967, A.C. demagnetization of rocks, *in* Collinson, D., Creer, K., and Runcorn, S., eds., Methods in paleomagnetism: New York, Elsevier, p. 256–286.

Manuscript Received 28 August 2005
Revised Manuscript Received 27 April 2006
Manuscript Accepted 30 April 2006

Printed in the USA